Structure of compound states in the chaotic spectrum of the Ce atom: Localization properties, matrix elements, and enhancement of weak perturbations

V. V. Flambaum, A. A. Gribakina, and G. F. Gribakin
School of Physics, University of New South Wales, Sydney, 2052, Australia

M. G. Kozlov
St. Petersburg Nuclear Physics Institute, Gatchina, St. Petersburg, Russia
(Received 23 December 1993)

The aim of the present paper is to analyze a realistic model of a quantum chaotic system: the spectrum and the eigenstates of the rare-earth atom of Ce. Using the relativistic configuration-interaction method the spectra and the wave functions of odd and even levels of Ce with $J = 4$ are calculated. It is shown that the structure of the excited states at excitation energies above 1 eV becomes similar to that of the compound states in heavy nuclei. The wave functions of the excited states are chaotic superpositions of the simple basis states (with the number of "principal" components $N \sim 100$), built of the $4f$, $6s$, $5d$, and $6p$ single-electron orbitals. The localization of the eigenstates on the energy scale is characterized by the spread width $\Gamma \sim ND$, where D is the average level spacing ($D \sim 0.03$ eV). The emergence of chaos in the spectrum and the dependence of the N and Γ parameters on the excitation energy are studied. The shape of the localization is shown to be Lorenzian around the maximum (principal components), whereas outside this region the squared components display a faster decrease, in agreement with the perturbation theory treatment of the band random matrix (BRM) model. The structure of the real interaction matrix is compared with that assumed in the BRM models. A formula expressing the mean-squared values of matrix elements between the eigenstates in terms of their parameters and single-particle occupancies is derived, and its applicability is checked with the results of numerical calculations. The hypothesis of a Gaussian distribution of the eigenstates' components and matrix elements between the eigenstates has been checked. The existence of the statistical (dynamical) enhancement of weak perturbations in systems with dense spectra is demonstrated.

PACS number(s): 31.20.Tz, 31.50.+w, 32.30.−r, 05.45.+b

I. INTRODUCTION

The aim of the present paper is to analyze a realistic model of quantum chaotic system: the spectrum and the eigenstates of the rare-earth atom of Ce. It is shown that the wave functions of the excited states are chaotic superpositions of basis states constructed of single-electron orbitals. We investigate the localization properties of the states and the dependence of parameters characterizing the structure of the chaotic eigenstates on their energy. A preliminary account of the present work has been given in [1]. The use of the realistic numerically solvable model provides a test for the applicability of the statistical approach to the calculation of the matrix elements between the chaotic states. The numerical calculations also show that the admixture of the states of different symmetry due to a weak perturbation in the system with dense chaotic spectrum is enhanced with respect to this admixture in a system with a rare "regular" spectrum (statistical enhancement). The results of the work can be extrapolated to other quantum systems: molecules, clusters, mesoscopic systems, and nuclei. A particularly intriguing question is the possibility of observing the statistical enhancement of the weak parity-nonconcerving interaction in chemical reactions, similar to that observed in nuclear reactions.

It is a well known fact that rare-earth atoms have very complicated spectra [2]. It originates from the open-shell configuration of their ground states and from the presence of several vacant electron orbitals in the immediate vicinity of the valence ones. Thus, if a large number of valence electrons n (in fact, $n = 4$, as in the Ce atom, can be well considered as "large") are distributed among those orbitals, it generates an exponentially large number of combinations, representing the basis of many-electron states of the system. Since these states have close energies, a dense spectrum emerges in the system.

The states in this spectrum can be classified by the values of the total angular momentum and parity J^π, where $J \sim n$. The states with different J^π do not interact with each other. However, the density of states with fixed J^π is still exponentially large, so that the average level spacing D for them is small compared to the residual interaction V. This interaction mixes up the basis states made from the single-electron orbitals, thus forming a complex pattern of the atomic energy levels. The levels obtained can hardly be classified using any of the coupling schemes, e.g., the LS one, because the fine structure intervals are much larger than D. The interaction of the state with the neighboring ones is large in V/D parameter and is completely nonperturbative. It is shown below that for a Ce atom the excited states in $J^\pi = 4^-$ and 4^+ manifolds are formed by strong mixing of about $N \sim 100$ basis states (principal components). The occupancies of the single-electron orbitals in such states are far from being

integer, and it is almost impossible to determine even the dominant nonrelativistic electron configuration for them.

The situation described above makes the spectrum of excited states of the rare-earth atoms very similar to the spectra of compound nuclei [3], though the compound states in nuclei are spread over a much greater number of principal components: $N \sim 10^4 - 10^6$. Their spectral properties were widely modeled using random-matrix theory and, in particular, the Gaussian orthogonal ensemble (GOE) (see, e.g., the review [4]). The GOE enables one to calculate the level spacing distribution (Wigner distribution) and to obtain other characteristics of energy-level fluctuations. The predictions of these models have been checked with numerous nuclei spectra and it seems natural that they also hold for the spectra of the rare-earth atoms. Indeed, the study of the nearest-neighbor level spacing distribution and some other fluctuation properties with the experimental spectra of Nd, Sm, and Tb (excitation energies of 2–4 eV, $D \sim 0.03$ eV) [5] showed good agreement with the predictions of the GOE.

Besides the statistical properties of the dense, chaotic energy spectrum, there is another and more important question: the structure of the corresponding eigenfunctions — compound states. This structure, and the number N of principal components in the first place, determines the magnitude of matrix elements between these states. As an impressive example of this one may consider parity-nonconserving phenomena in neutron-nucleus reactions, where the observed effect exceeds the naive single-particle estimate by orders of magnitude. To account for this the idea that the closely lying s and p resonances of the compound nucleus are mixed by the weak interaction has been put forward in [6] (see also [7]). If one supposes these states are constructed of about N principal components, which are mixed together in a random fashion, then the root-mean-square value of the matrix element between them is $M \propto 1/\sqrt{N}$. On the other hand, the spacing between nearest neighbors in the spectrum is $D \sim \Gamma/N$, where Γ is the so-called spread width of the single-particle component. Thus the admixture of the nearest state of opposite parity to a given one is $M/D \propto \sqrt{N}$. This factor determines the so-called *statistical* (or *dynamical*) *enhancement* of the weak interaction in the system.

To the best of our knowledge there has been only one paper [8] that examined statistical properties of the chaotic eigenstates of a rare-earth atom. In this work a sequence of 35 $J^\pi = 4^+$ energy levels of Ce lying at energy of $E = 2 - 3$ eV ($D = 0.027$eV) above the atomic ground state was considered. Statistically analyzing the contributions of the two leading configurations given in [2], the author concluded that these levels were random superpositions of some few basic states and the number of these states was estimated at $N \simeq 15$ (see Appendix A).

In contrast to the scarce information on the structure of chaotic states in real systems, there exist a great number of works studying different models, where properties of these states are investigated. The models include quantum kicked rotator (see, e.g., a review [9]) and ensembles of band random matrices (BRM's) ([10] is a comprehensive guide to the problem, from the pioneering work by Wigner [11] to the recent analytical results [12]). Initially the BRM model had been suggested as a model for the Hamiltonian matrix describing the mixing of basis states in a compound nucleus.

These models enable one to investigate the conditions for the emergence of quantum chaos and to study the *localization* of eigenstates. This property implies that the perturbation mixes the basis states locally and the components of a given eigenstate rapidly (exponentially, as usually assumed) vanish as one moves away from the center of the eigenstate. The typical scale of this decrease is called *the localization length.* This quantity is very similar to the number of principal components N, which makes the question of localization and the calculation of the localization length so relevant to the physical problems. However, there are only a few models which allow a deep analytical treatment, e.g., that of BRM's without leading monotonically increasing diagonal [12], and the requirement of the mathematical tractability usually contradicts to the reasonable physical requirements. Thus the absence of the leading diagonal disagrees with the fact that basis states can always be ordered according to their energies, and it is basically the energies of the states which make the mixing of distant components small (perturbation theory limit). In addition, apart from the usual assumption of the BRM models that the matrix elements are certain random variables with zero expectation and fixed variance, the whole bandlike structure may be considered only as a rough approximation to the real Hamiltonian matrix.

The Hamiltonian matrix of a real complex system in the basis of single-particle states is infinite, bound from below, and unbound from above. It is mostly irregular, and its properties, such as the spectral density of the eigenstates, the mean squares of matrix elements, and the number of basis states strongly mixed by perturbation, etc., are changing along the matrix (or with the excitation energy of states considered). Moreover, this matrix is unique. Hence one cannot perform any ensemble averaging, which is a key point of the random-matrix theories. The only possible averaging is that over the neighboring eigenstates. The question then is the following: to what extent do the properties of the chaotic eigenstates of this particular matrix agree with those commonly implied and used, e.g., for the description of the nuclear compound states?

The study of rare-earth atoms provides the possibility to investigate quantum chaos in a real and rather simple system. The number of principal components mixed by the perturbation for excitation energies above 1 eV is about 10^2 (compare it with $10^4 - 10^6$ in compound nuclei). It enables one to calculate these states numerically using the configuration-interaction (CI) approach and remaining well within the available computer facilities. Studying this model we trace how the chaos emerges starting from the very ground state. Then we study the characteristics of the chaotic eigenstates and their dependence on the excitation energy and calculate matrix elements between the compound states in order to com-

pare the results obtained with what one would expect from the statistical theory. It also gives a possibility to check various assumptions (such as the Gausian distribution of the components) made when analyzing chaotic eigenstates.

On the other hand, this study gives an insight into the structure of the excited states of the rare-earth atoms themselves. It yields better understanding of the manifestation of the correlation interaction and confirms the existence of the dynamical enchancement of the weak interaction in the spectra of rare-earth atoms [13].

The paper has the following structure. In Sec. II we consider the electronic structure of the Ce atom and examine the features of its experimental and calculated spectra. In Sec. III we analyze the structure of the Hamiltonian matrix and the localization properties of the chaotic eigenstates obtained from the matrix diagonalization in the CI scheme. The dependence of the parameters of the chaotic states on energy and their relation to the spectrum density are investigated. In Sec. IV we use the statistical theoretical approach to calculate the matrix element between the chaotic states and check the formulas obtained with the results of the numerical calculation of the transition matrix element between the chaotic states. In Sec. V we consider the mixing of chaotic states due to a weak perturbation. The existence of the statistical enhancement of the mixing coefficient is demonstrated and the corresponding enhancement factor is estimated. Section VI gives a brief summary of the results. In the Appendixes we analyze the statistics of the leading percentages, provide the details of the numerical CI calculation of the Ce levels, introduce the reduced density matrix operator, present the investigation of the eigenstates localization, including the perturbation theory approach to it, make comparisons of our realistic calculations for Ce with the approaches and results of the BRM models, and check the Gaussian character of the components' distribution.

II. THE STRUCTURE AND SPECTRUM OF THE CERIUM ATOM

A. Electronic structure of the Ce atom

The Ce atom has the atomic number of $Z = 58$ and it is the second one in a row of the rare-earth atoms. Its electronic structure consists of a Xe-like $1s^2 \ldots 5p^6$ core and four valence electrons. The atomic ground state belongs to the $4f5d6s^2$ valence configuration with $J^\pi = 4^-$. The ionization threshold of Ce is 5.539 eV and the binding energies of $5p_{3/2}$ and $5p_{1/2}$ electrons are 22 and 25 eV, respectively [14]. Therefore, the valence and the core electrons are well separated on the energy scale. It means that the excited states of Ce below the ionization threshold are formed by four valence electrons moving in the field of the core. Apart from generating the potential for the outer electrons the core screens (reduces) the Coulomb interaction between them. It will be shown below that the screening influences the average density of states in the spectrum.

The origin of the complicated and dense spectra of excited states in the rare-earth atoms is the existence of several orbitals in the immediate vicinity of the ground state. For lanthanides they are $4f$, $6s$, $5d$, and $6p$ orbitals, or in the relativistic notations $4f_{5/2}$, $4f_{7/2}$, $6s_{1/2}$, $5d_{3/2}$, $5d_{5/2}$, $6p_{1/2}$, and $6p_{3/2}$. It makes a total of $N_s = 32$ single-electron states. For Ce with $n = 4$ valence electrons there are about $(N_s)^n/n! \sim 4\times10^5$ possible many-electron states constructed of them. If one takes into account that there are about 20 different J^π manifolds, that each of the states is $2J + 1$ times degenerate ($2J + 1 \sim 10$ for an average J), and assumes that the states cover the energy range of 10 eV, the estimate for the average level spacing for fixed J states is $D \sim 0.005$ eV, or for the density $\rho \equiv D^{-1} \sim 2 \times 10^2$ eV^{-1}. We shall see below that the observed level density is several times smaller due to the selective population of some of the subshells, e.g., only one or two electrons can be found in the $4f$ subshell (not zero). Nevertheless, D is definitely much smaller than the spin-orbit interaction, or the residual interaction, which mixes up the configurations constructed of the single-electron states.

B. Level density and level spacing

To illustrate the above outlined picture let us examine the experimental spectra of Ce levels with $J^\pi = 4^-, 4^+$. We have chosen this value of the total angular momentum for two reasons. First, the Ce ground state is an odd level of $J = 4$. Second, these sequences are the best represented in [2], because $J = 4$ is close to the average (or the most probable) magnitude of the angular momentum one might expect of the four electrons distributed among the above listed orbitals.

Instead of searching for a way to average and plot the density of states $\rho(E)$,

$$\rho(E) = \sum_i \delta(E - E^{(i)}) \tag{2.1}$$

($E^{(i)}$ is the energy of the ith level), it is more instructive to examine the staircase plot for the cumulative number of levels:

$$N(E) = \int_{-\infty}^{E} \rho(E')dE' \ . \tag{2.2}$$

The density can be estimated from it as the slope of the curve, averaged over the level-to-level fluctuations of their positions. Figure 1 shows the $N(E)$ functions for 62 odd and 132 even levels of the $J = 4$ sequences and for 70 even levels with $J = 1$, available in [2]. There is a marked difference in the character of the curves for odd and even $J = 4$ levels. The odd one exhibits large energy gaps and corresponds to an average level spacing of about $D \simeq 0.067$ eV whereas the slope for the even levels rapidly increases to $D \simeq 0.0165$ eV and remains practically constant for the 15–85 levels. It will be shown below that the matrix elements of the interconfiguration residual interaction V are about 0.1 eV. Therefore, D for the

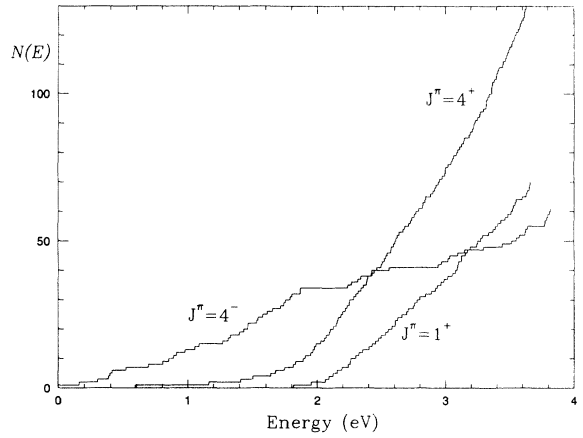

FIG. 1. Staircase plot of the cumulative numbers of $J^\pi = 4^-, 4^+, 1^+$ levels of Ce. Energies are taken from the tables [2].

odd levels in this part of the spectrum is just comparable to them, whereas D for the even levels is much smaller than V. It explains the difference between the irregular (odd) and the chaotic (even) behavior of the spectra. It is worth noting that the spectral properties of the $J^\pi = 1^+$ sequence are similar to those for the $J^\pi = 4^+$ one. The levels studied in [8] (3–37) and claimed chaotic there have $D \simeq 0.026$ eV, so that the condition $D \ll V$ is fulfilled.

In Fig. 2 the distribution of level spacings S for the levels 15–85 of the even $J = 4$ sequence is presented. It may be considered as the simpliest test of the chaotic structure of the Ce spectrum. Indeed, the shape of the histogram agrees well with the Wigner distribution $P(S) = (\pi S/2D^2)\exp(-\pi S^2/4D^2)$ with given $D = (E^{(85)} - E^{(15)})/70 \simeq 0.0165$ eV. This is confirmed by $\chi^2(10) = 6.6$ at 80% confidence level.

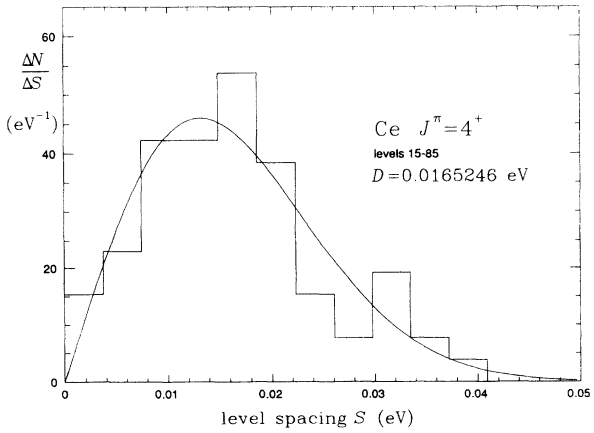

FIG. 2. Level spacing distribution for the $J^\pi = 4^+$ levels of Ce: experimental level spacings for 15–85 levels [2] (histogram) and the Wigner distribution $P(S) = (\pi S/2D^2)\exp(-\pi S^2/4D^2)$ with $D = (E_{85} - E_{15})/70 \simeq 0.0165$ eV.

C. CI calculations $J^\pi = 4^-, 4^+$ states of the Ce atom

As outlined above the goal of the present work is to investigate a realistic model of the quantum chaotic system. Hence the calculations we perform for the Ce spectra neither aim to reproduce the positions of particular energy levels nor to give assignments to the experimental data. Performing the *ab initio* calculations we are mostly interested to grasp the global features of the experimental spectra. It ensures the applicability of our conclusions on the chaotic properties of the states, obtained for the model, to the real atomic system.

The calculations were performed using the Hartree-Fock-Dirac (HFD) and the CI codes by Tupizin [15]. In the spirit of the CI approach we distinguish the Xe-like core and the four valence electrons above it. HFD code provided us with a basis of the single-electron orbitals for the core and valence electrons. The minimal basis for the calculation of the Ce spectrum included seven orbitals: $4f_{5/2}$, $4f_{7/2}$, $6s_{1/2}$, $5d_{3/2}$, $5d_{5/2}$, $6p_{1/2}$, and $6p_{3/2}$, since they all appear within the leading configurations of the Ce levels above 1.67 eV. The quality of the basis was estimated in the subsequent CI calculation. The main requirements it had to meet were the correct configurations of the lowest states in both even and odd $J = 4$ sequences and a reasonable order of the first few levels. We also checked the energy positions of the configurations' centers. The particular way of constructing the basis of single-electron orbitals is outlined in Appendix B.

The CI code is organized in the following way. Using the input list of the relativistic valence configurations of certain parity, it constructs all possible single-determinant states Ψ_i of them, corresponding to the given value of the projection of the total angular momentum of the atom M:

$$|\Psi_i\rangle = a^\dagger_{\nu_1} a^\dagger_{\nu_2} \dots a^\dagger_{\nu_n} |\Psi_0\rangle, \tag{2.3}$$

where $a^\dagger_\nu$ is the creation operator, its subscript ν denoting the single-electron $nljm$ states, $|\Psi_0\rangle$ is the atomic core state, and $\sum_1^n m = M$. The Hamiltonian matrix $H_{ik} = \langle\Psi_i|\hat{H}|\Psi_k\rangle$ in the single-determinant basis is evaluated using the single-electron HFD orbitals.

In Table I the configurations used for the CI calculations of the $J^\pi = 4^-, 4^+$ are shown. For each parity they include all possible ways of distributing four electrons among seven valence orbitals with a restriction that there are one or two $4f$ electrons and no more than three $5d$ electrons. The omitted configurations have higher energies and essentially do not influence the spectrum at excitation energies of a few eV. Each of the nonrelativistic configurations includes all possible relativistic configurations and produces quite a large number of single-determinant states (see Table I). The matrix element H_{ik} between the single-determinant states vanishes if the states Ψ_i and Ψ_k differ by the states $nljm$ of more than two electrons. Therefore, the H_{ik} matrix has a very sparse structure. There are only 6.4% and 6.25% of the nonzero matrix elements in it for the odd and the even levels, respectively.

TABLE I. Configurations and basis sets used for calculating the $J^\pi = 4^-, 4^+$ levels of Ce.

Levels	Nonrelativistic configurations	No. of relativistic configurations	No. of single-determinant $M = 4$ states	No. of states in the $J = 4$ subspace	Energy of the configurations with $J = 4$ (eV)[a]
4^-	$4f6s^25d$	4	8	4	1.21
	$4f6s5d^2$	6	74	29	2.26
	$4f^26s6p$	6	66	23	3.30
	$4f5d^3$	8	101	36	4.71
	$4f5d6p^2$	12	122	51	6.07
	$4f^25d6p$	12	335	104	6.34
	$4f6s6p^2$	5	22	13	7.13
total	7	53	728	260	
4^+	$4f^26s^2$	3	6	3	1.63
	$4f6s5d6p$	8	97	42	3.37
	$4f5d^26p$	12	225	83	4.27
	$4f6s^26p$	3	4	3	4.52
	$4f^26s5d$	6	111	36	4.65
	$4f^26p^2$	9	84	31	6.04
	$4f^25d^2$	9	255	78	8.98
total	7	50	782	276	

[a]The average energies of the configurations (mean values of the diagonal Hamiltonian matrix elements) are given with respect to the lowest odd eigenstate.

Due to the conservation of the angular momentum the perturbation, however strong it is, cannot completely mix the basis states Ψ_i. The mixing takes place within the subspace of states characterized by definite values of the angular momentum (eigenstates of the $\hat{J}^2$ operator). Therefore, a new basis of Ψ_{Ji} states has been constructed prior to the Hamiltonian diagonalization (see Appendix B for details):

$$\Psi_{Ji} = \sum_{i'} A_{Ji,i'} \Psi_{i'} \ , \tag{2.4}$$

$$\hat{J}^2 \Psi_{Ji} = J(J+1)\Psi_{Ji} \ ,$$

$$\langle \Psi_{J'i} | \hat{H} | \Psi_{Jk} \rangle = \sum_{i',k'} A^*_{J'i,i'} H_{i'k'} A_{Jk,k'} = H^{(J)}_{ik} \delta_{JJ'} \ . \tag{2.5}$$

Each of the submatrices $H^{(J)}_{ik}$ has a much greater number of nonzero matrix elements (about 60% in our calculations). In principle, all states of the Ψ_{Ji} basis are coupled by the residual interaction, possibly in higher orders if the first order matrix element (2.5) between them is zero. However, the eigenvalue problem for the $H^{(J)}_{ik}$ matrix is much simpler numerically because the rank of the submatrix is considerably lower than that of H_{ik}.

D. The Ce spectrum: Loss of good quantum numbers and transition to chaos

Solving the eigenvalue problem for the $H^{(J)}_{ik}$ matrix, the eigenvalues $E^{(i)}$ and eigenfunctions $\Psi^{(i)}$ of a given J^π symmetry are obtained:

$$\sum_{k'} H^{(J)}_{kk'} C^{(i)}_{k'} = E^{(i)} C^{(i)}_k \ ,$$

$$\Psi^{(i)} = \sum_k C^{(i)}_k \Psi_{Jk} \ , \tag{2.6}$$

where $C^{(i)}_k$ are the components of the eigenstates in terms of the Ψ_{Jk} basis. The results of the diagonalization for $J^\pi = 4^-, 4^+$ are presented in Figs. 3 and 4. The staircase plot of the cumulative number of the eigenvalues $E^{(i)}$ is compared with the spectrum of the diagonal matrix elements of the Hamiltonian (a) and with the experimental spectrum (b). All calculated energies are given with respect to the energy of the lowest odd eigenvalue, which is set to zero together with the experimental $J^\pi = 4^-$ ground state.

The $H^{(J)}_{ii}$ expectation values correspond to the energies of the many-electron Ψ_{Ji} basis states (we denote them as E_i). One may consider them as the positions of the energy levels in the zeroth approximation, when the interaction with other states is neglected. Indeed, they take into account the kinetic energy, the interaction with the atomic core and the Coulomb interaction of the valence electrons. The configuration interaction leads to the "straightening" of the spectrum [especially clear in the sequence of even levels Fig. 4(a)]. The variations of the $H^{(J)}_{ii}$ level density are smoothed down on a scale of about 2 eV. It will be shown in Sec. III that this value is of the order of the spread width Γ of the eigenstates over the energies of the basis states. This effect is a direct result of the level repulsion. It strongly manifests in the parts of the spectra where the average level spacing is much smaller than the typical matrix element $H^{(J)}_{ik}$ $(i \neq k)$ between the configurations (see Sec. III). The repulsion of levels is also quite noticeable near the edges of the of the spectrum, where it shifts the eigenvalues down (lower-energy edge) or up (higher-energy edge) relatively to the $H^{(J)}_{ii}$ energies. However, we would like to stress the leading role of the Hamiltonian diagonal, which governs the average slope of the staircase eigenvalue plot.

It is very important that the calculated spectra of odd

and even levels qualitatively agree with the experimental data [Figs. 3(b) and 4(b)]. Despite apparent distinctions in the positions of the levels, the calculation reproduces the substantial difference between the odd and the even sequences. We would like to point out once more that adjusting the single-electron basis one can better fit either the odd or the even states. However, in order to calculate them both accurately within the *ab initio* approach would require an uncomparably greater basis of configurations. Our certainty is based on the experience of the many-body perturbation theory calculations in heavy atoms (see [16]). It shows that in order to reproduce the level energies with an accuracy of about 1% one should take into account the core polarization by the valence electrons and the screening of the Coulomb interaction of the valence electrons and between the valence electrons and the atomic core. Roughly speaking, the core polarization lowers the energy levels, and the screening reduces the Coulomb repulsion between the electrons, making energy intervals smaller.

The influence of these effects on the positions of the individual levels in the dense spectra of the rare-earth atoms must be enhanced due to the small level spacing. As is known both the core polarization and the screening involves the electron excitations into the continuum. In the CI approach this means a huge additional number of configurations, including those with excitations from the core. In principle, one can take them into account in a semiempirical way, introducing a model core potential and screening factors for the Coulomb integrals.

One may understand the role of these effects from the comparison of the experimental and calculated spectra of the even levels [Fig. 4(b)]. The experimental spectrum density is about 1.5 times larger than the calculated one at $E \sim 2-4$ eV. The energies of omitted valence electron configurations place them at much higher energies, thus not increasing the density in the low-energy region. We believe that it is the screening which might be responsible for the "softening" of the calculated spectra.

Besides the smoothing scale Γ there is another important energy scale: the scale of the level spacing D (several hundredths of an eV). On this scale a switch takes place from the Poisson distribution of the spacings between the diagonal Hamiltonian matrix elements to the Wigner distribution of the eigenvalue spacings (Fig. 5). The fluctuation properties of the energy levels are probably the

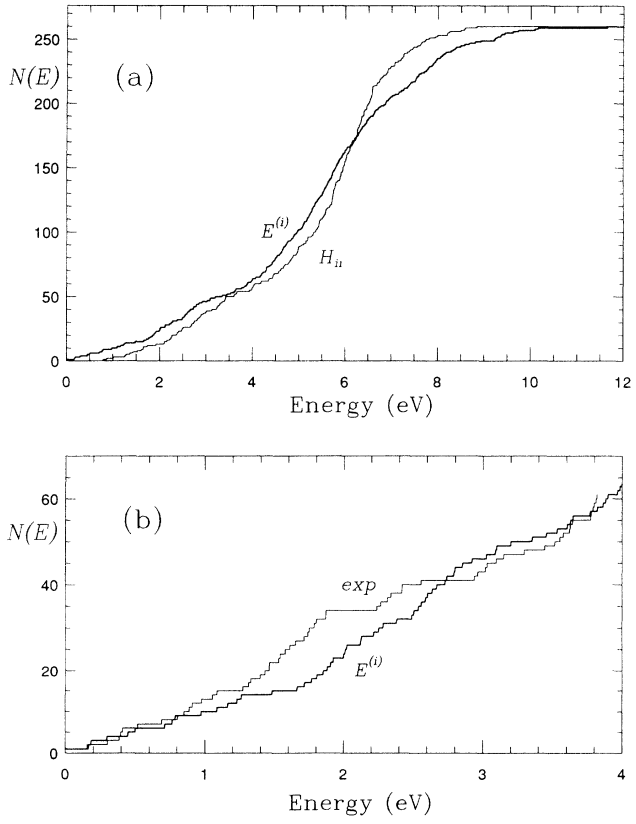

FIG. 3. The results of the CI calculation of the spectrum of the odd levels of Ce ($J = 4$). The staircase plot for the cumulative numbers of eigenvalues $E^{(i)}$ (thick line) is compared with (a) the diagonal matrix elements of the Hamiltonian matrix $H_{ii}^{(J)}$ (thin line) and (b) the experimental $J^\pi = 4^-$ energy levels of Ce (thin line) [2].

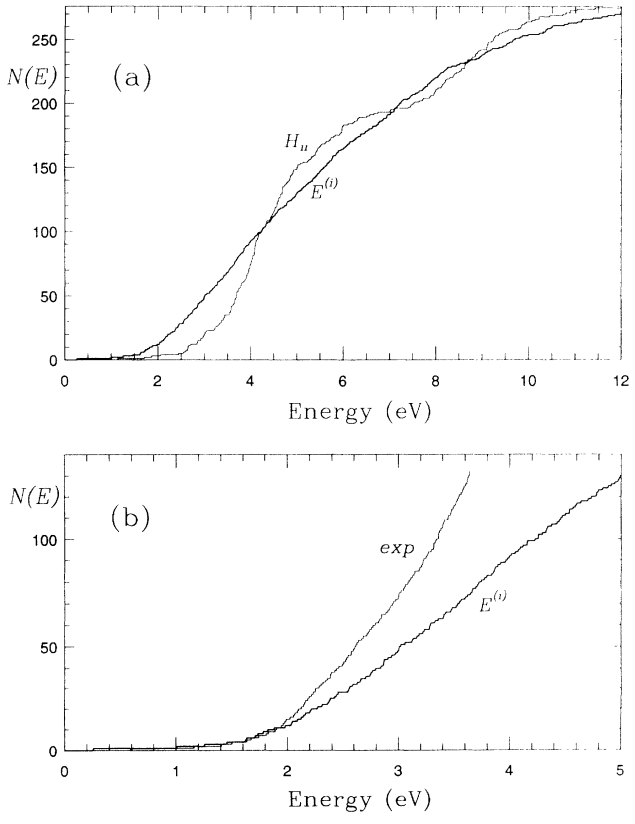

FIG. 4. The results of the CI calculation of the spectrum of the even levels of Ce ($J = 4$). The staircase plot for the cumulative numbers of eigenvalues $E^{(i)}$ (thick line) is compared with (a) the diagonal matrix elements of the Hamiltonian matrix $H_{ii}^{(J)}$ (thin line) and (b) the experimental $J^\pi = 4^+$ energy levels of Ce (thin line) [2].

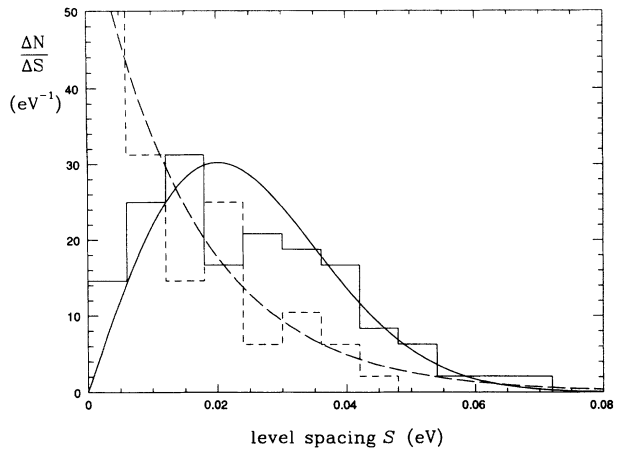

FIG. 5. Level spacing distributions for the diagonal matrix elements of the Hamiltonian $H_{ii}^{(J)}$ (dashed line histogram) and the eigenvalues (solid line histogram) for the 20–100 even $J = 4$ levels. They are compared with the Poisson distribution $P(S) = D^{-1}\exp(-S/D)$ ($D = 0.0155$ eV) (dashed curve) and with the Wigner distribution ($D = 0.0252$ eV) (solid curve), yielding $\chi^2(7) = 7.85$ and $\chi^2(9) = 8.17$, respectively.

best understood and the most universal feature of the chaotic spectra [4,5]. Since the level spacing distribution essentially involves the short-range correlations in level positions, it is the least model dependent characteristic, and the predictions of the simplest Gaussian orthogonal ensemble are valid for most of the cases studied. Without going into further details let us note that the observed slight deviations from the standard distributions partially result from the energy dependence of the locally averaged level density. The latter is especially prominent for the diagonal energies.

The third energy scale is the energy spanned by the configurations included in the CI calculations (about 10 eV). In our case it is comparable to the natural scale of the ionization limit of about 5.5 eV. The finite number of configurations included produces a decrease of the calculated density of states above 6 eV for the odd levels and above 4 eV for the even ones. First, this is in disagreement with the experimental data. Second, it contradicts the simple physical picture that a number of single-electron orbitals available, and hence the number of their many-electron combinations, increase with the energy. Therefore, only the low-energy parts (the left halves, roughly) of the calculated spectra behave in a realistic way and reproduce the features of a real system. This is the extent to which our results are physically correct. Beyond that the CI calculation is just a numerical investigation of yet another quasi-random-matrix model. However, above the ionization threshold the multiconfigurational eigenstates form a dense spectrum of autoionizing resonances. In an analogy with the compound states in nuclei these states could have very small widths. We suppose that the approach used in this paper can give an insight into that spectral region as well.

The investigation of the energy spectrum which emerges in the CI calculations does not prove the chaotic structure of the eigenstates. A detailed consideration of this question will be carried out in Sec. III. Prior to that we examine the dependence of the orbital occupancies n_{nlj} on the energy of the states (Figs. 6–8). The occupancies are obtained from the diagonal matrix elements of the reduced density matrix (see Appendix C). Since the ratio of the occupancies of the fine structure sublevels $j = l \pm \frac{1}{2}$ is close to the statistical $\frac{l+1}{l}$ (see Fig. 8), the sums $n_{nl} = n_{nll-1/2} + n_{nll+1/2}$ are presented for the $4f$, $5d$, and $6p$ orbitals.

It is clearly seen from Figs. 6 and 7 that the occupancies for the first several levels are very close to integer. Indeed the lowest odd states can be unambiguously associated with the $4f6s^25d$ (states 1,3,6,7) or $4f6s5d^2$ (states 2,4,5,8,9,...) configurations and the $4f^26s^2$ and $4f6s5d6p$ configurations form the low-lying levels of the even manifold. However, with the energy increasing the occupancies start to deviate noticeably from integer values. In order to distinguish better between systematic trends and the fluctuations, the window-averaged values of the occupancies are presented (thick curves). The plots again reveal a substantial difference between the structure of the odd and even levels. In the former case the fluctuations are considerably larger and one can easily find numerous states clearly belonging to the well-defined

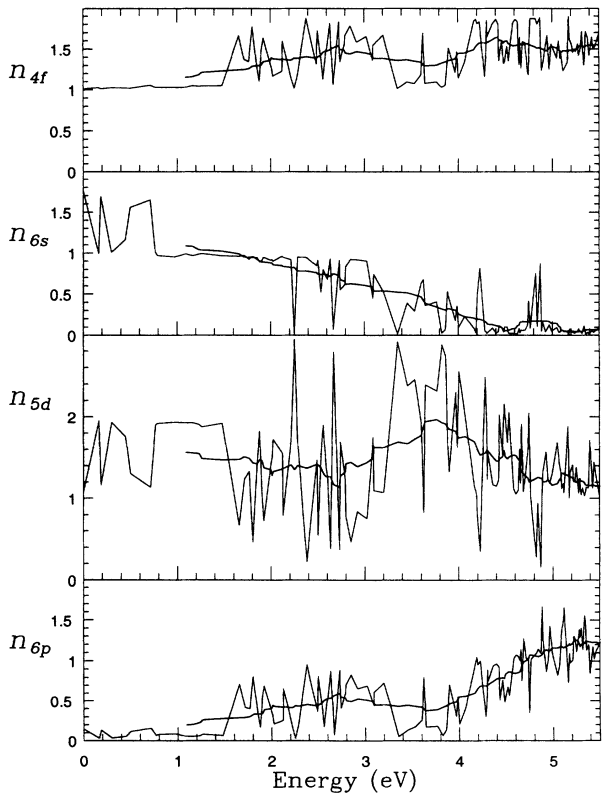

FIG. 6. The dependence of the orbitals' occupancies on the energy of the eigenstate for the 1–130 odd $J = 4$ levels. The thick line shows the occupancies averaged over the 19 neighboring levels.

nonrelativistic configurations (e.g., $4f5d^3$ between 2 and 4 eV). It does not mean that these states are "simple." They are still build up of a large number of basis states, belonging to different relativistic configurations (Table I).

The matrix elements of the residual interaction $H_{ik}^{(J)}$ $(i \neq k)$, which mix the basis states, have essentially the same magnitudes for the odd and even levels (Sec. III). This means that the difference between the behavior of the odd and even occupancies originates from the difference of the level density for these cases. Figure 4 shows that for the even levels the dense and gapless spectrum with average spacing of about $D \sim 0.025$ eV arises at $E > 2$ eV, whereas the odd spectrum (Fig. 3) at $E < 4$ eV is much rarer: $D \sim 0.08$ eV. The latter value is close to the typical mixing matrix element, thus preventing a complete mixing of the interleaved states of different configurations in this energy region. However, when the density of the odd spectrum rapidly increases beyond 4.5 eV the amplitude of the fluctuations drops down to the values characteristic of the even spectrum.

On the whole, we observe that the chaotic mixing of the basis states emerges first within particular nonrelativistic electron configurations. As long as the admixture of other configurations is small, one can still classify the states according to their leading percentages. With the energy of the states increasing, this possibility vanishes and the total angular momentum and parity J^π remain the only good quantum numbers. We shall see below that instead of quantum numbers one can describe these eigenstates in the statistical way in terms of the number of the principal components N they are built of and the spread width Γ, which specifies the energy range of the basis states strongly mixed in a chaotic eigenstate. This approach is used, for instance, in nuclei for the description of the compound resonances. It justifies the use of the term *compound states* for the chaotic eigenstates in the rare-earth atom spectrum, and both terms will be used hereafter.

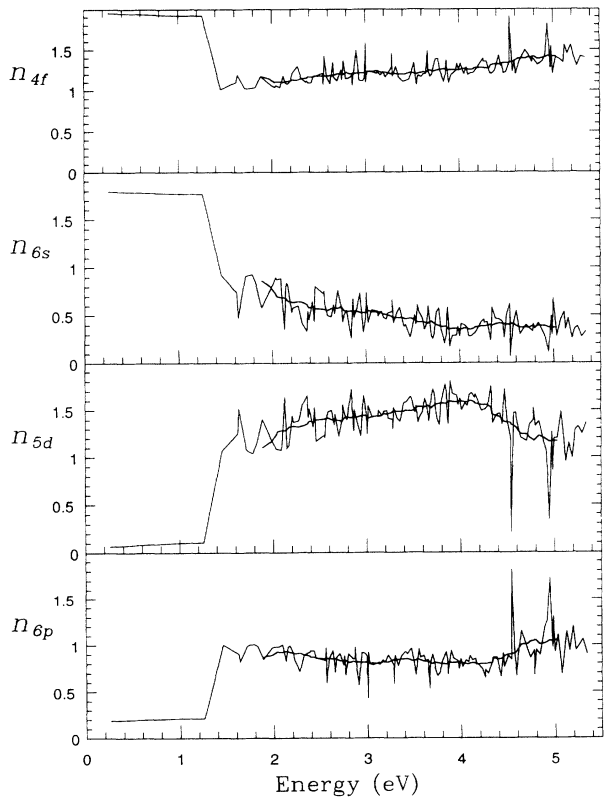

FIG. 7. The dependence of the orbitals' occupancies on the energy of the eigenstate for the 1–140 even $J = 4$ levels. The thick line shows the occupancies averaged over the 19 neighboring levels.

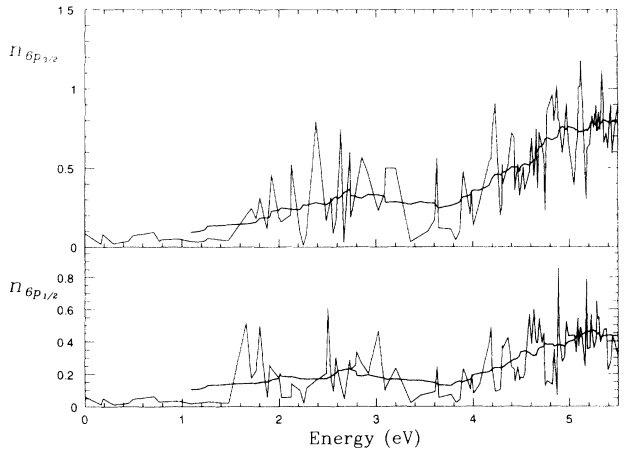

FIG. 8. The dependence of the $6p_{1/2}$ and $6p_{3/2}$ occupancies on the energy of the eigenstate for the 1–130 odd $J = 4$ levels. The thick line shows the occupancies averaged over the 19 neighboring levels.

III. STRUCTURE OF THE CHAOTIC EIGENSTATES

A. The Hamiltonian matrix

After studying the spectrum of eigenvalues and before investigating the eigenstates, let us examine the characteristic features of the Hamiltonian matrix $H_{ij}^{(J)}$ which produces them both. So far we have seen the distribution of the diagonal matrix elements [Figs. 3(a) and 4(a)]. The basis states Ψ_{Ji} are arranged in the way that $H_{ii}^{(J)} \equiv E_i$ increases monotonically with i. The rate of this increase corresponds to the average spacing of about $D \sim 0.035$ eV between the energies of the basis states. Apart from the effects of level repulsion discussed above the spectrum of eigenvalues essentially follows the main diagonal of the Hamiltonian matrix.

The main feature of the off-diagonal matrix elements $H_{ij}^{(J)}$ is that their dependence upon the level numbers i, j is almost random. It occurs because the basis states belonging to the different configurations are strongly interspersed on the energy scale and the basis states Ψ_{Ji}

TABLE II. Statistical characteristics of the off-diagonal elements of the Hamiltonian matrix used in the CI calculations of the $J^\pi = 4^-,4^+$ levels of Ce.

	$J = 4$ odd, 260×260 matrix		$J = 4$ even, 276×276 matrix	
Quantity	Whole matrix	$H_{ij} \neq 0$ only[a]	Whole matrix	$H_{ij} \neq 0$ only[a]
$\overline{H_{ij}^2}$ [b] (eV^2)	0.0072	0.0128	0.0076	0.0130
$\sqrt{\overline{H_{ij}^2}}$ (eV)	0.085	0.113	0.087	0.114
$\overline{H_{ij}}$ (eV)	-4×10^{-4}	-8×10^{-4}	-1×10^{-5}	-2×10^{-5}
No. of H_{ij} $(i < j)$	33670	18987	37950	22220
ρ [c] (eV^{-1})	50		40	
Γ [d] (eV)	2.3		1.9	

[a]This means that the small matrix elements $|H_{ij}| < 10^{-6}$ a.u.$\simeq 2.7 \times 10^{-5}$ eV are omitted.
[b]Here $H_{ij} \equiv H_{ij}^{(J)}$, i.e., we investigate the Hamiltonian matrix (2.5) in the Ψ_{Ji} basis.
[c]For the level densities ρ we use values averaged over the 5–7 eV energy range for the odd spectrum and over 3–6 eV for the even one (Fig. 15).
[d]The spread width Γ is calculated as $\Gamma = 2\pi\rho V^2$, where the characteristic value of the squared nondiagonal matrix element V^2 is set to $\overline{H_{ij}^2}$.

themselves are rather complex linear combinations of the simple single-determinant states. Figure 9 shows the mean squared values of $\overline{H_{ij}^2}$ [from now on we omit the angular momentum index (J) since all basis-dependent characteristics will be given with respect to the Ψ_{Ji} basis]. They are obtained for $i, j = 10, 20, \ldots$ using the window averaging with a square $W \times W$ window $(W = 19)$. The same procedure applied to H_{ij} produced the values $|\overline{H_{ij}}| \sim \left(\overline{H_{ij}^2}\right)^{1/2} / \sqrt{W^2}$, which one would expect if the matrix elements have random signs. The "ragged terrain" observed in Fig. 9 shows a weak trend of the matrix elements to group along the main diagonal (a little more distinct in the CI matrix for the even levels). Though it is physically apparent that the matrix elements between distant configurations become very small, this happens when the configurations differ by the states of at least two electrons or when one electron is excited to a high-lying Rydberg or continuous spectrum state. In general it would require larger excitation energies than those spanned by our bases.

The overall statistical information about the off-diagonal matrix elements of the CI matrices for the odd and even $J = 4$ levels is presented in Table II. It yields practically equal root-mean-squared values of the off-diagonal matrix elements for both cases: $\left(\overline{H_{ij}^2}\right)^{1/2} \simeq 0.085$ eV. Taking into account the number of different matrix elements involved in averaging (the matrices' upper triangles contain about 3.5×10^4 matrix elements) one obtains an estimate for the mean off-diagonal matrix element: $\overline{H_{ij}} \sim \left(\overline{H_{ij}^2}\right)^{1/2} / \sqrt{3.5 \times 10^4} \simeq 4.5 \times 10^{-4}$ eV. This value is consistant with the numerical ones (see Table II), which also proves the random-sign character of H_{ij}.

It is quite interesting to analyze the distribution of

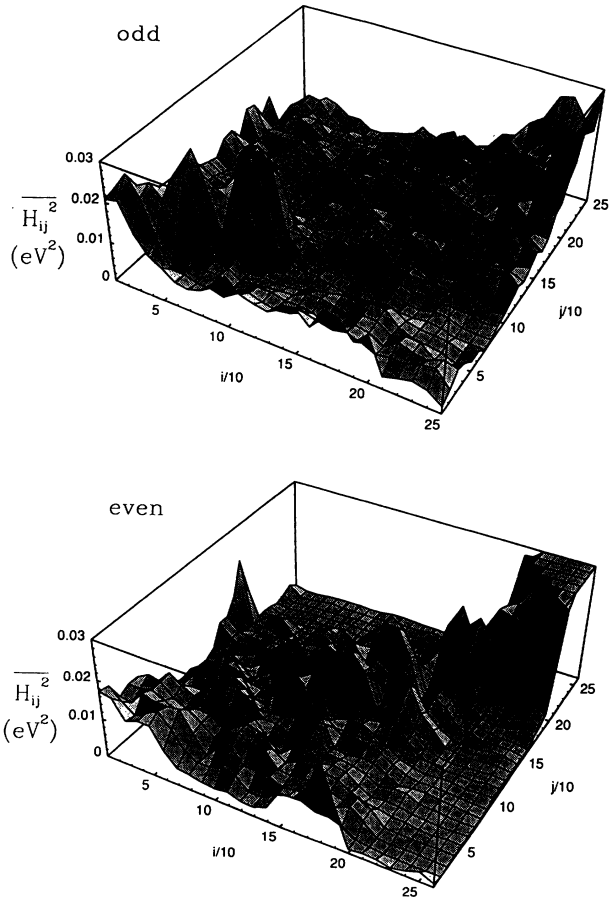

FIG. 9. The dependence of the mean-squared nondiagonal matrix element $\overline{H_{ij}^2}$ on the basis states' numbers i and j for the $J^\pi = 4^-,4^+$ Hamiltonian matrices (the 19 × 19 window averaging used). The values averaged over the whole matrix are 0.0072 eV^2 (odd) and 0.0076 eV^2 (even).

the matrix elements. Its logarithm is presented in Fig. 10. The distributions for the odd and even matrices are remarkably similar apart from the small vertical shift due to the different size of the matrices. Both histograms show very large numbers of small matrix elements since the central bin accumulates as many as the half of the matrix elements. For larger H_{ij} the distribution can be approximated by a simple exponential formula $\frac{\Delta N}{\Delta H} \propto |H_{ij}|^{-1/2} \exp(-|H_{ij}|/V)$. This is shown in Fig. 10 with $V = 0.12$ eV. This value is close to the root mean square of the off-diagonal matrix element averaged over the nonzero matrix elements. The agreement observed proves once more that the values given in Table II provide reliable estimates of the basis states' mixing matrix element in this problem.

Examining the H_{ij} matrix we see that about half of the matrix elements are very small (Table II). If one uses this estimate and assumes (roughly) that the matrix has a bandlike structure, then the magnitude of the bandwidth can be estimated (the bandwidth b is defined so that $H_{ij} \neq 0$, if $|i-j| \leq b$ and $H_{ij} = 0$ otherwise). It gives $b \simeq 80$. A more accurate estimate (Appendix E) yields $b \simeq 60$ for the odd matrix and $b \simeq 50$ for the even one. This type of information may be useful when making comparisons between the results of the CI calculations for the real system (the spectrum of the Ce atom) with various predictions obtained from the BRM model [10–12,17].

For example, we can easily prove the leading role of the diagonal matrix elements H_{ii} (i.e., the zero approximation energies of the basis states) in forming the spectrum. If the increase of the diagonal matrix elements can be neglected (the BRM without leading diagonal), then the distribution of the eigenvalues is described by the semicircle law [11,18]:

$$\rho(E) = \frac{1}{4\pi V^2 b}\sqrt{8bV^2 - E^2}\,, \tag{3.1}$$

where V^2 is the mean square of the off-diagonal matrix element ($V^2 \equiv \overline{H_{ij}^2}$ in our case). Using the mean value for the nonzero matrix elements $\overline{H_{ij}^2} \simeq 0.013$ eV^2 one obtains for the "diameter" of the semicircle $\Delta E = 2(8bV^2)^{1/2} \sim 5$ eV (for some average value of $b = 55$). It would be the characteristic energy range spanned by the levels due to their repulsion. We indeed checked this figure numerically, diagonalizing H_{ij} with H_{ii} set to zero (though the level density showed some deviations from the semicircle law). As seen from Figs. 3 and 4, the true spectrum of the odd and even levels extends over twice as large energy region.

B. Parameters of the chaotic states: Principal components

The eigenstates corresponding to the odd and even $J = 4$ levels of Ce are represented in Fig. 11 by their components C_j against the energy E_j of the basis states. The eigenstates shown approximately cover the lower half

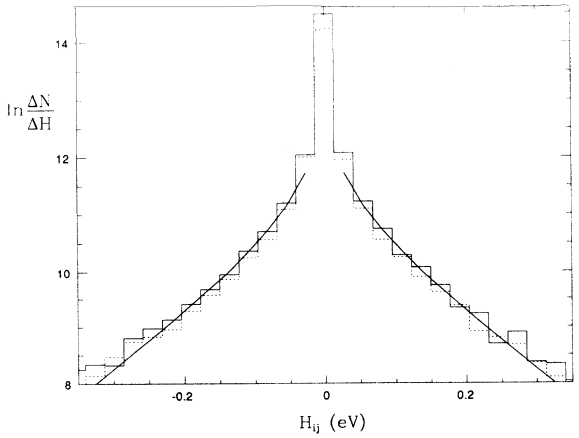

FIG. 10. The distribution of the nondiagonal matrix elements of the Hamiltonian matrix for the $J^\pi = 4^-$ (dashed line histogram) and $J^\pi = 4^+$ (solid line histogram) levels of Ce. A simple approximation $\frac{\Delta N}{\Delta H} = 2.56 \times 10^4 |H_{ij}|^{-1/2} \exp(-|H_{ij}|/V)$ with $V = 0.12$ eV is shown (solid line).

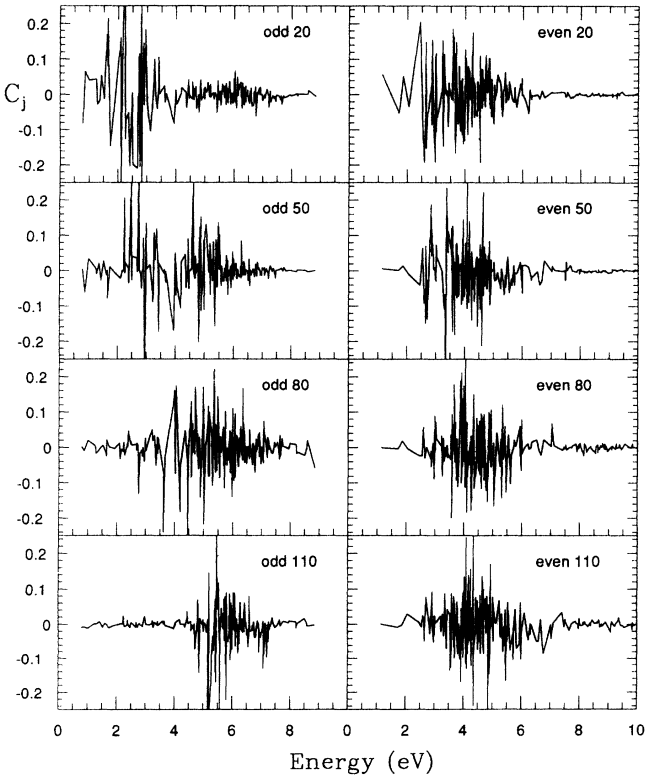

FIG. 11. The odd and even $J = 4$ eigenstates of Ce. Shown are the eigenstates' components C_j in terms of the Ψ_{Ji} basis states vs the energies E_j of basis states ($E_j \equiv H_{jj}^{(J)}$). One can clearly see the localization of the eigenstates and the shift of the eigenstates towards higher energies, following the increase of the eigenvalues. Note the marked difference between the lower (20 and 50) odd and even eigenstates.

of the spectra. One can see that even relatively low-lying states are distributed among a large number of components. Two effects can be clearly observed in the figure. First, the states are well localized on the energy scale, i.e., the components contributing to a particular eigenstate are mainly confined within an energy interval of about $2-3$ eV. This behavior agrees with the existence of a characteristic spread width Γ, which determines the energy range within which the basis states are strongly mixed by the perturbation (or, alternatively, the range of eigenvalues to which a given basis state noticeably contributes). The additional "splashes" of the components outside this range are caused by large values of particular matrix elements, e.g., those between the states of the $4f^26s^2$ and $4f^26p^2$ configurations (lying 5.5 eV apart). However, this admixture of distant components is still relatively small. The second effect is the regular shift of the large components' bunch following the increase of the eigenstate energy. The latter means the localization of components around the eigenstate they represent.

The localization of the chaotic eigenstates in various models is characterized by the parameter L, called the localization length, or the inverse quantity, called the inverse participation ratio (see, e.g., [12,18] and Appendix E). It is usually associated with the exponential decrease of the components $|C_j^{(i)}| \propto \exp(-|i-j|/L)$. Describing the compound states in real systems, say, in the heavy nuclei, another parameter, namely, the number of principle components N, is used. It can be defined as the inverse mean-squared root $\left(\overline{C_j^{(i)2}}\right)^{-1/2}$ of the principal components. One may believe that a relation $L \sim N$ is valid, though there are no direct proofs that the number of large $C_j^{(i)2}$ and their asymptotic behavior are governed by the same parameter. This is probably true for the BRM models without the leading diagonal, where the bandwidth b is the only parameter (we assume that the matrix has infinite size, as relevant to the physical problem). The presence of the increasing diagonal provides an additional dimensionless parameter V/D. Thus a difference between the above defined L and N arises (see Appendixes D and E).

In order to study the distribution of the components of the chaotic eigenstates on the energy scale in a more detailed way let us consider the *strength function* introduced by Wigner [11]:

$$\rho_w(E,j) = \sum_i C_j^{(i)2}\delta(E-E^{(i)}) \ . \tag{3.2}$$

$\rho_w(E,j)$ is the level density weighted with the probabilities to find the jth basis state in the eigenstates. If one performs the averaging, Eq. (3.2) turns into

$$\overline{\rho_w(E,j)} = D^{-1}\overline{C_j^{(i)2}} \equiv D^{-1}w(E_j;E,\Gamma,N) \ , \tag{3.3}$$

where D is the locally averaged level spacing: $D^{-1} \equiv \overline{\rho(E)} = \overline{\sum_i \delta(E-E^{(i)})}$ and $E \simeq E^{(i)}$. The averaging above can be performed in two ways. The first one requires an ensemble of random matrices, producing the eigenvalues $E^{(i)}$ and eigenstates $C_j^{(i)}$, i.e., it is an ensemble averaging. The second type of averaging is performed over the neighboring eigenstates i or components j. This can be done for the unique matrix (or real system) and represents the spectral averaging. In the spirit of the ergodic hypothesis we believe they should yield identical results for most of the physically reasonable quantities. It is natural that throughout the paper only the second type of averaging is used. Namely, we employ the window averaging over the W successive levels, thus allowing for (and neglecting) the possible $W^{-1/2}$ fluctuations.

In Eq. (3.3) a function $w(E_j;E,\Gamma,N) \equiv \overline{C_j^{(i)2}}$ has been introduced. This function describes the structure of the chaotic eigenstates in terms of the number of principal components N and the width Γ within which the eigenstates contain a noticeable portion (about N^{-1}) of the basis state j. Apparently, a relation $ND \simeq A\Gamma$ must be valid, where $A \sim 1$ is a constant depending on the actual shape of the w function and on the exact definition of N and Γ. The most important property of $w(E_j;E,\Gamma,N)$, suggested by the models [3,11] and the numerical calculations (see below), is that it essentially depends on the difference E_j-E between the basis state energy and the energy of the eigenstate, and not just on the number j of the eigenstate. Moreover, w is a symmetric function of E_j-E (if one neglects the smooth energy dependence of N and Γ). Therefore, it shows the dependence of the mean-squared components of a given eigenstate of E energy on the *energies* E_j of the basis states. This point of view seems more appropriate for the present investigation than considering w as the contribution of a given component j to the various eigenstates.

The normalization of the eigenstates $\sum_j C_j^{(i)2} = 1$ imposes the following requirement on $w(E_j;E,\Gamma,N)$:

$$\sum_j w(E_j;E,\Gamma,N) = 1$$

$$\rightarrow \quad \int w(E_j;E,\Gamma,N)\frac{dE_j}{D} = 1 \ , \tag{3.4}$$

where we assumed that w is a smooth function of E_j, so that the sum over j can be replaced by the integral over dE_j/D. It is a consequence of Eq. (3.4) that $w \sim N^{-1}$ around its maximum, i.e., at $|E_j-E| < \Gamma$. The integration in (3.4) can be formally extended from $-\infty$ to $+\infty$ provided w drops rapidly enough.

The mean-squared components $\overline{C_j^{(i)2}}$ obtained by means of averaging over the W neighboring eigenstates ($W=19$) are shown in Fig. 12 as functions of E_j. It is interesting to observe how $\overline{C_j^{(i)2}}$ evolves for the odd eigenstates with the increase of the level number. The maximum of $\overline{C_j^{(i)2}}$ for the odd levels around $i=20$ is about 0.03, implying $N \sim 30$ principal components. With the increase of the level number the magnitude of $\overline{C_j^{(i)2}}$ successively decreases and becomes the same as for the even levels around $i > 100$. In contrast with that $\overline{C_j^{(i)2}}$ is already about 0.01 for the even levels with $i \gtrsim 50$. This difference is another manifestation of the difference revealed earlier between the odd and even spectra (Secs. II B and II C). Since each of the 40 bins used to calculate

the $\overline{C_j^{(i)2}}$ contains about 10^2 components from 19 eigenstates, fluctuations of about 10% might be expected. The observed rate of fluctuations agrees with the existence of a smooth curve w behind the histograms shown. However, there are several effects which distort the symmetric and smooth shape of $\overline{C_j^{(i)2}}$.

The first one is a regular low-energy dispacement of the energy eigenvalue with respect to the maximum of $\overline{C_j^{(i)2}}$ (it corresponds to the second order perturbation theory energy shift $\Delta E_i = \sum_j \frac{V_{ij}^2}{E_i - E_j}$). This is a manifestation of the uncompensated level repulsion near the lower edge of the spectrum [Figs. 3(a) and 4(a)]. The accompanying effect is the skewness of the $\overline{C_j^{(i)2}}$ for the lower eigenvalues, which is especially noticeable for the 20th even state (the even eigenstates around $i = 20$ contain about 50 main components, which inevitably causes such skewness). The latter also occurs since the basis states set is bounded from below. Accordingly, both effects gradually disappear with increasing eigenvalue number. Other effects include enhanced fluctuations for the small N lower odd levels and some nonstatistic deviations of the $\overline{C_j^{(i)2}}$ shape, causing the appearence of additional "shoulders" beside the central maximum. Nevertheless, we believe that in order to clearly describe the main features of the chaotic eigenstates one may neglect all the above mentioned effects. Still, we will allow for the first of them (the displacement of the maximum), assuming that an additional parameter ΔE, the magnitude of the displacement, can be introduced into $w(E_j; E, \Gamma, N)$. The question now is the following: what is the actual analytical form of $w(E_j; E, \Gamma, N)$ that we may use to fit the numerical data in Fig. 12?

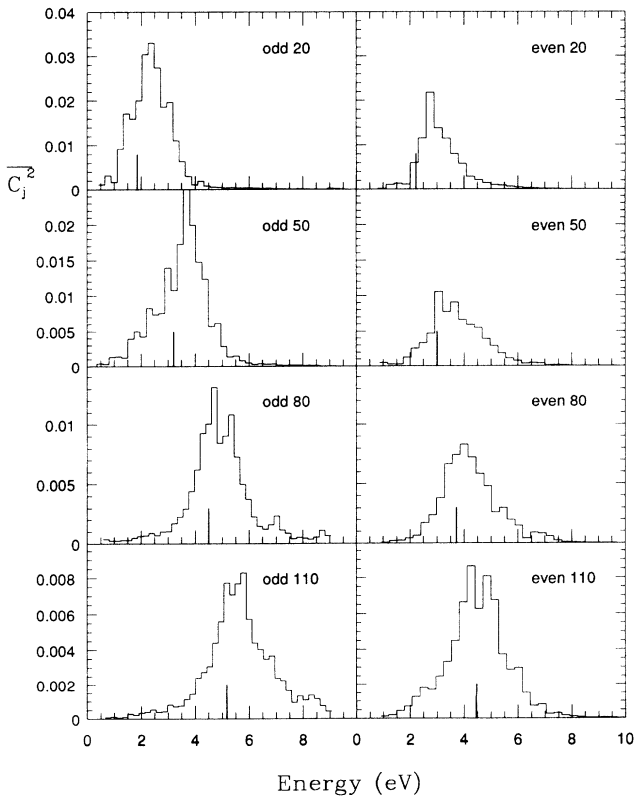

FIG. 12. The dependence of the mean-squared component $\overline{C_j^2}$ on the energy of the basis state E_j (the strength function) for the odd and even eigenstates of Ce. The squared components $C_j^{(i)}$ were first distributed on their energies $E_j - E^{(i)}$. Then the averaging was performed within each of the 40 bins over the $C_j^{(i)}$ of the 19 neighboring eigenstates. Long thick ticks show the positions of the corresponding energy eigenvalues.

In [11] an integral equation for the strength function $\overline{\rho_w}$ for the infinite BRM with the leading diagonal has been obtained. It has been shown that in the case of $\frac{V^2}{D^2 b} \ll 1$ the localization of the eigenstates is described by a simple Lorenzian curve

$$w(E_j; E, \Gamma, N) = \frac{1}{N} \frac{\Gamma^2/4}{(E - E_j)^2 + \Gamma^2/4} \qquad (|E - E_j| < Db) \ , \quad (3.5)$$

where the spread width is $\Gamma = \frac{2\pi V^2}{D}$ and the number of principal components $N = \frac{\pi\Gamma}{2D}$ is introduced in the way that $w = N^{-1}$ at the maximum. Equation (3.5) describes $\overline{C_j^{(i)2}}$ within the band. The condition $\frac{V^2}{D^2 b} \ll 1$ is equivalent to $\Gamma \lesssim Db$, i.e. the spread width of the state is supposed to be less than the energy width of the band. Accordingly, the normalization condition (3.4) is automatically fulfilled. It is quite remarkable that Eq. (3.5) coincides with the results of the model description of the strength function in the case of a level interacting with an equidistant spectrum of other levels by a constant matrix element V [3]. Though Eq. (3.5) describes a nonperturbative mixing of states, it reproduces the perturbation theory result at $Db > |E - E_j| > \Gamma$: $\overline{C_j^{(i)2}} \simeq \frac{V^2}{(E - E_j)^2}$.

Beyond the bandwidth Db, Eq. (30) of [11] predicts a modified exponential drop:

$$w(E_j; E, \Gamma, N) \propto \exp\left\{-2\xi \ln\left(\xi e^{-1}\sqrt{2q^{-1}\ln[\xi/\sqrt{q}]}\right)\right\}, \quad (3.6)$$

where

$$\xi = \frac{|E - E_j|}{Db} \ , \quad q = \frac{V^2}{D^2 b} \ . \quad (3.7)$$

Note that this formula is different from the asymptotic solution (35a) in [11], since the latter is incorrect. The derivation of the correct expression (3.6) is given in Appendix D together with the perturbation theory consideration of the behavior of distant components. It is shown there that the form of Eq. (3.6) reflects the feature of the BRM that the coupling of the distant components happens via higher order perturbation theory terms. Thus the exponential decrease predicted by the formula above is essentially governed by the energy bandwidth Db (if one neglects the logarithmic factor) and does not depend

explicitly on the number of principal components N or the spread width Γ.

As seen in Fig. 12 the whole energy range spanned by the CI calculations is only a few times larger than the widths of the $\overline{C_j^2}$ maxima. Therefore, one cannot study the mixing of distant components in detail in our numerical model, and we concentrate below on the description of the large principal components. In order to find the parameters N and Γ of the chaotic eigenstates the averaged squared components $\overline{C_j^2}$ obtained from the CI calculations have been fitted with the Lorenzian curves $w(E_j; E+\Delta E, \Gamma, N)$ using the least-squares method. The fits for the 80th odd and even levels are shown in Fig. 13. They yield $N = 86$, $\Gamma = 1.58$ eV and $N = 118$, $\Gamma = 1.64$ eV for the odd and even levels, respectively.

Despite an overall reasonable agreement of the Lorenzian fits with $\overline{C_j^2}$, one may notice that the latter shows a faster decrease at the wings of the central maximum. It is a manifestation of the transition from Eq. (3.5) to another form, like that of Eq. (3.6). In order to check this and to estimate the quality of the fit, two other fits have been tried. Introducing the shape function $f(\epsilon)$: $w(E_j; E + \Delta E, \Gamma, N) = N^{-1} f(\epsilon)$, where $\epsilon \equiv \frac{E_j - E - \Delta E}{\Gamma}$, they are characterized by $f(\epsilon) = (1 + 4\epsilon^2)^{-2}$ (squared Lorenzian fit) and $f(\epsilon) = \exp\left(1 - \sqrt{1 + 4\epsilon^2}\right)$ (interpo-

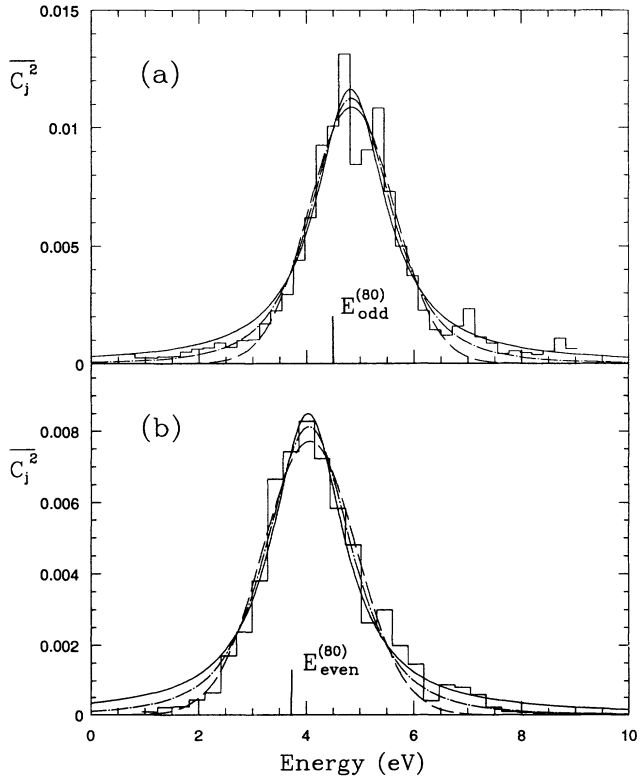

FIG. 13. Fitting the $\overline{C_j^2}$ with $w(E_j; E, N, \Gamma)$ for the 80th (a) odd and (b) even eigenstates. The least-squares Lorenzian (solid curve), squared Lorenzian (dash-dotted curve), and interpolation exponential (dashed curve) fits are shown.

TABLE III. Comparison of the Lorenzian, squared Lorenzian, and interpolation exponential fits of $\overline{C_j^2}$ for the 80th odd and even eigenstates of Ce.

		Quality of fit [a]		
Level	Bins	Lorenzian	Squared Lorenzian	Interpolation exponential
80 odd	$13 - 27$ [b]	6.9	4.7	5.6
	$1 - 40$ [c]	21.6	10.6	14.7
80 even	$6 - 18$ [b]	1.5	2.3	2.2
	$1 - 40$ [c]	2.1×10^3	22.8	43.7

[a]The values given below are the normalized variances $N_{\rm bin} \times \left(\frac{\overline{C_j^2} - w(E_j; E+\Delta E, \Gamma, N)}{\overline{C_j^2}}\right)^2$ averaged over the 40 bins of the $\overline{C_j^2}$ histogram ($N_{\rm bin}$ is the number of C_j falling into the bin, $N_{\rm bin} \sim 10^2$). If the distribution of C_j within each bin is Gaussian, the variance for the "perfect" fit must be equal to 2.

[b]The maximum region $\overline{C_j^2} > 0.1 \left(\overline{C_j^2}\right)_{\rm max}$.

[c]The whole energy range.

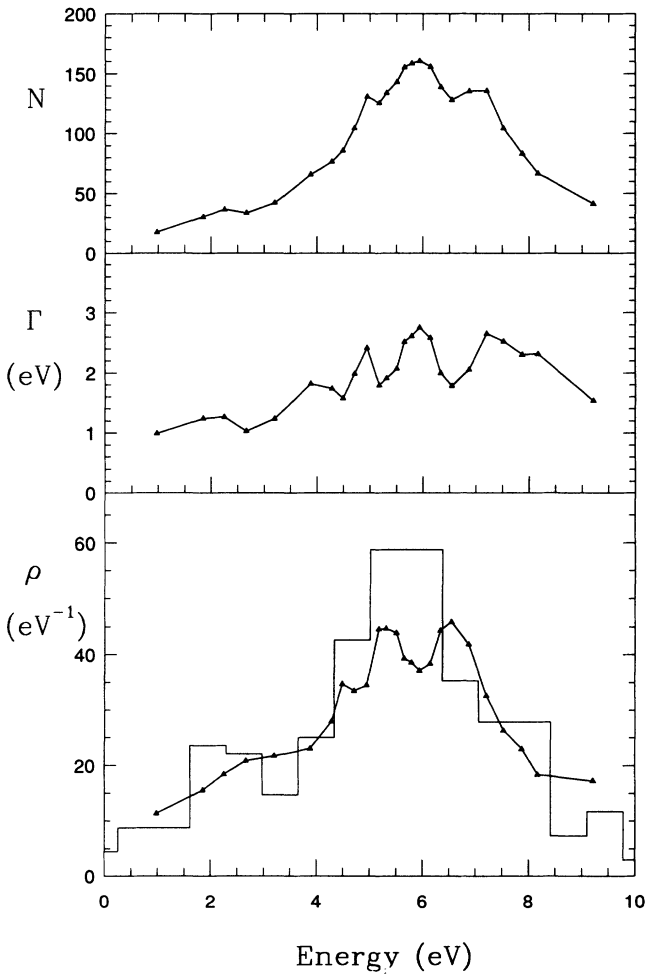

FIG. 14. The number of principal components N and the spread width Γ for the $J^\pi = 4^-$ eigenstates. Solid triangles show the data obtained from the Lorenzian least-squares fit of $\overline{C_j^2}$. In the lower part the inverse level spacing $D^{-1} = \frac{2N}{\pi\Gamma}$ (triangles) is compared with the calculated level density ρ (histogram) for the $J^\pi = 4^-$ states.

lation exponential fit), while $f(\epsilon) = (1 + 4\epsilon^2)^{-1}$ corresponds to the pure Lorenzian fit (3.5). The squared Lorenzian shape takes into account the fact that outside the bandwidth the coupling of states happens by means of the next, second, order of perturbation theory. The interpolation exponential fit accounts for the same effect, roughly mimicking the behavior of Eq. (3.6) at $|\epsilon| > 1$: $f(\epsilon) \propto \left(-\frac{2|E-E_j|}{\Gamma}\right)$ (in our numerical example $\Gamma \sim Db \sim 2$ eV). Both non-Lorenzian fits are shown in Fig. 13. They are remarkably close to each other in the 4 eV range around the maximum.

The quality of the fits is analyzed in Table III for the maximum region $\overline{C_j^2} > 0.1\left(\overline{C_j^2}\right)_{\max}$ and for the whole energy range. In the first case one cannot see much difference between the fits. Apparently, the fluctuations for the 80th odd level exceed the limits allowed by the Gaussian statistics of components (the latter assumption is analyzed in Appendix E). However, the slow drop of the Lorenzian curve becomes evident when the normalized variances are analyzed for the whole energy range. From this point of view the best result is achieved with the squared Lorenzian fit. One should keep in mind that the average number of the C_j components in each bin is about 130. Therefore, a deviation of the $\overline{C_j^2}$ wings from the Lorenzian shape is statistically credible. It is necessary to mention that one can discover other systematic features in Fig. 13 which contribute to the difference between the calculated $\overline{C_j^2}$ and the fits, e.g., the shoulders on the right side of the main maximum. They are caused by the preferential mixing of some configurations and, probably, by the variations of the basis states density.

Despite the overestimation of the contribution of distant components, one may regard the achieved fit of the $\overline{C_j^2}$ maximum with the Lorenzian curve as fairly reasonable. The values of N and Γ obtained by fitting the window-averaged $\overline{C_j^{(i)2}}$ ($i = 10, 20, 30, \ldots$) with the Lorenzian curves are shown in Figs. 14 and 15. One can see that the parameters of the chaotic states vary considerably with the energy of the states. This is especially true for the number of the principal components, whereas the spread width displays smaller variations for both odd and even levels. According to the model calculations [3,11] the magnitude of the spread width can be estimated as $\Gamma = 2\pi V^2/D = 2\pi\rho V^2$. The values presented in the bottom line of Table II refer to the energies of 5–7 eV (odd) and 3–6 eV (even) and are in good agreement with those obtained from the fit (see Figs. 14 and 15).

The validity of the Lorenzian fit is checked in Figs. 14 and 15 (lower graphs) in another way. There we compare the level density ρ obtained from the eigenvalue spectrum with the inverse level spacing found from the normalization condition for the Lorenzian fit: $D^{-1} = \frac{2N}{\pi\Gamma}$. The agreement observed is a nontrivial fact since one might expect that the normalization condition (3.4) involves the level spacing between the basis state energies E_j rather than that between the eigenstates. Figures 3(a) and 4(a) give evidence that the spectral densities of the basis states and the eigenstates differ noticeably. However, the typical spread width of the eigenstate is largely comparable to a typical energy scale of the deviation between the two densities. Thus an averaging (smoothing) of the basis state density takes place, producing the D^{-1} values close to the eigenvalue density. Since the spread width Γ is a rather slowly varying function of energy, it is essentially the density of states which governs the behavior of the number of the principal components: $N = \frac{\pi\Gamma}{2D} = \frac{\pi}{2}\rho\Gamma$.

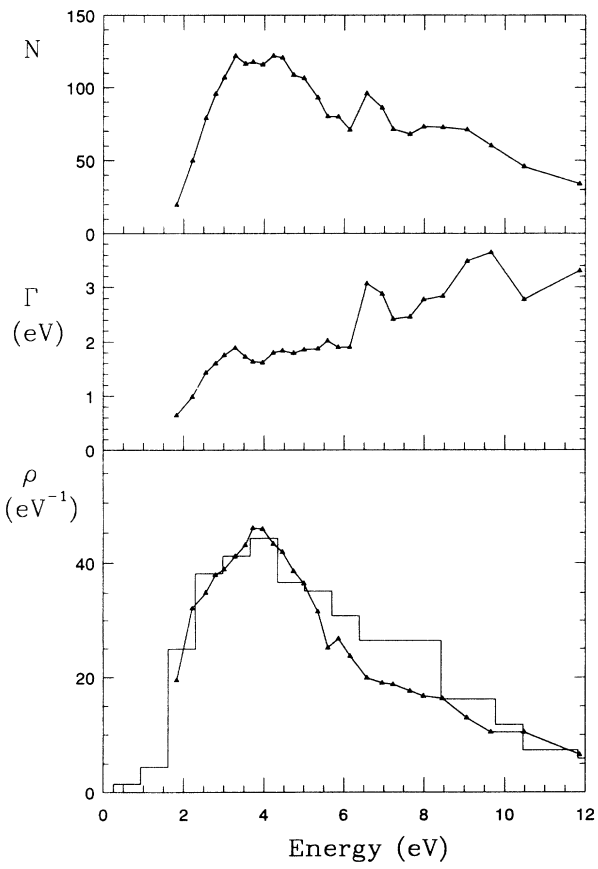

FIG. 15. The same as in Fig. 14, but for the $J^\pi = 4^+$ states.

IV. MATRIX ELEMENTS BETWEEN THE CHAOTIC STATES: STATISTICAL DESCRIPTION OF CHAOS

The preceding section presented an account of the properties of the chaotic eigenstates in the dense spectrum of the Ce atom. It has been shown that they are superpositions of a large number of basis states. The latter are mixed in such a way that the mean-squared value of the jth component $\overline{C_j^2}$ is described by the function $w(E_j; E, N, \Gamma)$, where E is the energy of the eigenstate and N and Γ are the number of principal components and the spread width, respectively. We now proceed to the calculation of the matrix elements between chaotic eigenstates. In doing so we aim to compare the statis-

tical approach to the calculation of the matrix element with the results of direct numerical calculations. This is a stringent test for both the assumptions used in the analytical calculation of the matrix element (Sec. IV A) and for the validity of the above given description of chaotic states.

A. Calculation of the mean-squared matrix element between the chaotic states

In the calculation of the matrix element between the chaotic eigenstates we follow the main ideas of [19–21], where a statistical approach to the calculation of the matrix element between compound states has been proposed. Suppose the states $|1\rangle$ and $|2\rangle$ are chaotic (in the sense of Sec. III) superpositions of large number of basis states

$$|1\rangle = \sum_i C_i^{(1)}|i\rangle, \qquad |2\rangle = \sum_i C_j^{(2)}|j\rangle \ . \tag{4.1}$$

The matrix element of an operator $\hat{M}$ is given by

$$M_{21} = \langle 2|\hat{M}|1\rangle = \sum_{ij} C_j^{(2)*} C_i^{(1)} \langle j|\hat{M}|i\rangle \ . \tag{4.2}$$

Since the matrix element between the compound states strongly varies from level to level, averaging over the states $|1\rangle$ and $|2\rangle$ is to be performed to obtain a typical value of M_{21}. This averaging is performed assuming the chaotic and uncorrelated distributions of the components

$$\overline{C_i^{(1)}} = \overline{C_j^{(2)}} = \overline{C_j^{(2)*} C_i^{(1)}} = 0 \ , \tag{4.3}$$

which results in the zero mean matrix element $\overline{M}_{21} = 0$. In the absence of the ensemble of random matrices and the ensemble of corresponding eigenstates and in the spirit of Sec. III we understand (4.3) as a window average over the set of neighboring eigenstates. The size of the window is chosen to embrace a large number of states W in order to make the relative fluctuations as small as $W^{-1/2}$. On the other hand, W is assumed to be smaller than the characteristic scale at which a variation of the eigenstates' parameters (N, Γ) takes place. Handling the numerical data of the CI calculations we stick to this type of averaging throughout the paper, and it is also used below for the numerical estimation of the matrix elements between the chaotic states. The statistical independence of the $C_i^{(1)}$ and $C_j^{(2)}$ components is ensured by the use of the states of different symmetry for $|1\rangle$ and $|2\rangle$.

Averaging the square of the matrix element (4.2) one obtains

$$\overline{|M_{21}|^2} = \sum_{ij} \overline{C_j^{(2)2}}\ \overline{C_i^{(1)2}} \langle j|\hat{M}|i\rangle\langle i|\hat{M}^\dagger|j\rangle \ , \tag{4.4}$$

where we again used the statistical properties of the components:

$$\overline{C_k^{(1)*} C_i^{(1)}} = \overline{C_i^{(1)2}}\delta_{ik} \ , \qquad \overline{C_j^{(2)*} C_l^{(2)}} = \overline{C_j^{(2)2}}\delta_{jl} \tag{4.5}$$

($C_i^{(1)}$ and $C_j^{(2)}$ are assumed real). It becomes apparent from (4.4) that the magnitude of the mean-squared matrix element between the chaotic eigenstates essentially depends on the squared components distributions. In most of applications $\hat{M}$ is either a single-body (external field) or a two-body (interparticle interaction) operator. Below we concentrate on the former case, whereas the latter is considered in [20].

If $\hat{M}$ is a single-electron operator $\hat{M} = \sum_{\alpha\beta}\langle\alpha|\hat{m}|\beta\rangle a_\alpha^\dagger a_\beta$ (α, β denote the single-electron states, $\hat{m}$ is the operator in the space of the single-electron states), it is convenient to express its matrix elements in terms of the matrix elements of the density matrix operator $\hat{\rho}_{\alpha\beta} = a_\alpha^\dagger a_\beta$,

$$M_{21} = \langle 2|\hat{M}|1\rangle = \sum_{\alpha\beta}\langle\alpha|\hat{m}|\beta\rangle\langle 2|a_\alpha^\dagger a_\beta|1\rangle = \sum_{\alpha\beta} m_{\alpha\beta}\rho_{\alpha\beta}^{(21)} \ , \tag{4.6}$$

where $\rho_{\alpha\beta}^{(21)} \equiv \langle 2|\hat{\rho}_{\alpha\beta}|1\rangle$ is the matrix element of the density matrix operator. The superscript (21) reminds one that this matrix element corresponds to the $1 \to 2$ transition and the operator should be rather called a *transition matrix* rather than a density matrix. The complex conjugation of the transition matrix element yields $\left(\rho_{\alpha\beta}^{(21)}\right)^* = \rho_{\beta\alpha}^{(12)}$.

The magnitude of $\rho_{\alpha\beta}^{(21)}$ determines the "weight" of the $\beta \to \alpha$ single-electron transition $\langle\alpha|\hat{m}|\beta\rangle$ in M_{21}. In contrast with the very large number of many-electron basis components the number of single-electron orbitals involved in the compound state is small. This makes the formalism of the density matrix operator quite appropriate for the description of the matrix elements between compound states.

If $|2\rangle = |1\rangle$ the transition matrix turns into a usual density matrix $\rho_{\alpha\beta}^{(11)} = \langle 1|a_\alpha^\dagger a_\beta|1\rangle$ and its diagonal matrix element yields the occupancy of the the single-electron state α in the many electron state $|1\rangle$: $\rho_{\alpha\alpha}^{(11)} = \langle 1|a_\alpha^\dagger a_\alpha|1\rangle \equiv \langle 1|\hat{n}_\alpha|1\rangle \equiv n_\alpha$ ($0 \le n_\alpha \le 1$).

Since the mean value of the matrix element between chaotic states is zero, it follows from (4.6) that $\overline{\rho_{\alpha\beta}^{(21)}} = 0$. The mean square of the matrix elements is expressed as

$$\overline{|M_{21}|^2} = \sum_{\alpha\beta} |m_{\alpha\beta}|^2 \overline{|\rho_{\alpha\beta}^{(21)}|^2} \ . \tag{4.7}$$

This formula is obtained from (4.6) with a supposition that the transitions between different pairs of single-electron states are uncorrelated: $\overline{\rho_{\alpha\beta}^{(21)}\rho_{\mu\nu}^{(21)*}} = \delta_{\alpha\mu}\delta_{\beta\nu}\overline{|\rho_{\alpha\beta}^{(21)}|^2}$. One can easily check that the latter is consistent with the assumptions (4.5) and that the formula (4.7) for $\overline{|M_{21}|^2}$ directly follows from (4.4) if $|i\rangle, |j\rangle$ are the basis states given by (2.3). Thus the mean-squared matrix elements of the density matrix operator determine the mean-squared matrix elements of other single-electron operators between the chaotic states. Accordingly, we consider below the case $\hat{M} = \hat{\rho}_{\alpha\beta}$.

Equation (4.4) then yields

$$\overline{|\rho^{(21)}_{\alpha\beta}|^2} = \sum_{ij} \overline{C^{(2)2}_j}\ \overline{C^{(1)2}_i} \langle j|a^\dagger_\alpha a_\beta|i\rangle\langle i|a^\dagger_\beta a_\alpha|j\rangle$$
$$= \sum_{ij} w_1(E_i) w_2(E_j) \langle j|a^\dagger_\alpha a_\beta|i\rangle\langle i|a^\dagger_\beta a_\alpha|j\rangle \ , \quad (4.8)$$

where $w_1(E_i) \equiv w(E_i; E^{(1)}, N_1, \Gamma_1)$ and $w_2(E_j) \equiv w(E_j; E^{(2)}, N_2, \Gamma_2)$ are the characteristic functions which describe the dependence of the mean-squared components on the energies E_i, E_j of the basis states. These functions depend on the energies $E^{(1,2)}$ and parameters N, Γ of the chaotic eigenstates.

Suppose the states $|i\rangle, |j\rangle$ are the many-electron basis states given by Eq. (2.3). Then for the fixed j there is only one state $|i\rangle = a^\dagger_\beta a_\alpha|j\rangle$, which gives a nonzero contribution to the sum (4.8). The energy of this state is determined by $E_i = E_j + \varepsilon_\beta - \varepsilon_\alpha = E_j + \omega_{\beta\alpha}$, where ε_α and ε_β are the single-particle energies of the electron states α and β. Therefore, the double sum (4.8) is reduced to

$$\overline{|\rho^{(21)}_{\alpha\beta}|^2} = \sum_j w_1(E_j + \omega_{\beta\alpha}) w_2(E_j) \langle j|a^\dagger_\alpha a_\beta a^\dagger_\beta a_\alpha|j\rangle$$
$$= \sum_j w_1(E_j + \omega_{\beta\alpha}) w_2(E_j) \langle j|\hat{n}_\alpha(1-\hat{n}_\beta)|j\rangle \ , \quad (4.9)$$

where the operator equality $a^\dagger_\alpha a_\beta a^\dagger_\beta a_\alpha = -a^\dagger_\alpha a_\alpha a^\dagger_\beta a_\beta + a^\dagger_\alpha a_\alpha = \hat{n}_\alpha(1-\hat{n}_\beta)$ $(\alpha \neq \beta)$ is used to express the matrix elements of the operators $a^\dagger$ and a in terms of the operators $\hat{n}_\alpha \equiv a^\dagger_\alpha a_\alpha$ of the number of particles. Alternatively, one can say that (4.9) follows from (4.8) after the summation over the complete set of $|i\rangle$ states is performed taking into account the energy conservation relation $E_i = E_j + \omega_{\beta\alpha}$.

Further simplifications are possible if one assumes that the occupancies of the single-electron states are slowly varying functions of the energy. Then the matrix element of the $\hat{n}_\alpha(1-\hat{n}_\beta)$ operator in (4.9) can be replaced with its average value $\sum_j w_2(E_j)\langle j|\hat{n}_\alpha(1-\hat{n}_\beta)|j\rangle = \langle n_\alpha(1-n_\beta)\rangle_2$ [note that $\sum_j w_2(E_j) = 1$ is the normalization condition]. The latter quantity is the mean value of the occupancy times the "emptiness" for the chaotic state $|2\rangle$ averaged over a number of neighboring levels. Extracting it from behind the sum in Eq. (4.9) we obtain

$$\overline{|\rho^{(21)}_{\alpha\beta}|^2} = \langle n_\alpha(1-n_\beta)\rangle_2 \sum_j w_1(E_j + \omega_{\beta\alpha}) w_2(E_j) \ . \quad (4.10)$$

Following the simple models provided in [3,11] and in agreement with the results of Sec. III we assume that the strength function $w(E_j; E, N, \Gamma)$ can be presented as

$$w(E_j; E, N, \Gamma) = N^{-1} f(\epsilon), \quad \epsilon = \frac{E_j - E}{\Gamma}, \quad f(0) = 1 \ , \quad (4.11)$$

where $f(\epsilon)$ is a universal symmetrical bell-shaped function with a width of about 1, which describes the localization of the eigenstate in terms of the basis components. Though its exact analytical form does not matter at all for the present calculation, the possible examples are the Lorenzian $f(\epsilon) = (1+4\epsilon^2)^{-1}$, or the squared Lorenzian $f(\epsilon) = (1+4\epsilon^2)^{-2}$ shapes, which were probed in Sec. III in connection with the real Ce eigenstates.

Having in mind to replace the summation over j in (4.10) by the integration over dE_j/D_2 (D_2 is the local average level spacing in the vicinity of the compound state $|2\rangle$), we do so for the normalization condition for $w(E_j; E, N, \Gamma)$ first:

$$\sum_j w(E_j; E, N, \Gamma) = 1 \quad \rightarrow \quad \int w(E_j; E, N, \Gamma) \frac{dE_j}{D} = \frac{1}{ND} \int_{-\infty}^{+\infty} f\left(\frac{E_j - E}{\Gamma}\right) dE_j = \frac{\Gamma}{ND} \int_{-\infty}^{+\infty} f(\epsilon) d\epsilon = 1 \ . \quad (4.12)$$

The last integral in (4.12) is a dimensionless quantity of about 1, which depends upon the choice of $f(\epsilon)$. If we denote it by $A \equiv \int f(\epsilon) d\epsilon$, the normalization condition will take the form of

$$A \frac{\Gamma}{ND} = 1 \ . \quad (4.13)$$

The sum in (4.10) is now calculated as follows:

$$\sum_j w_1(E_i + \omega_{\beta\alpha}) w_2(E_j) = \int w(E_j + \omega_{\beta\alpha}; E^{(1)}, N_1, \Gamma_1) w(E_j; E^{(2)}, N_2, \Gamma_2) \frac{dE_j}{D_2}$$
$$= \frac{1}{N_1 N_2} \int f\left(\frac{E_j + \omega_{\beta\alpha} - E^{(1)}}{\Gamma_1}\right) f\left(\frac{E_j - E^{(2)}}{\Gamma_2}\right) \frac{dE_j}{D_2} \ . \quad (4.14)$$

Let us now define a function $\tilde{\delta}(\Gamma_1,\Gamma_2,\Delta)$:

$$\tilde{\delta}(\Gamma_1,\Gamma_2,\Delta) \equiv \frac{1}{A^2\Gamma_1\Gamma_2}\int f\left(\frac{E+\Delta}{\Gamma_1}\right) f\left(\frac{E}{\Gamma_2}\right) dE \ . \tag{4.15}$$

Using (4.12) and (4.13) and the symmetry $f(-\epsilon)=f(\epsilon)$ one can easily check the following properties:

$$\int_{-\infty}^{+\infty} \tilde{\delta}(\Gamma_1,\Gamma_2,\Delta)\, d\Delta = 1 \ , \tag{4.16a}$$

$$\tilde{\delta}(\Gamma_1,\Gamma_2,-\Delta) = \tilde{\delta}(\Gamma_1,\Gamma_2,\Delta) \ , \tag{4.16b}$$

$$\tilde{\delta}(\Gamma_2,\Gamma_1,\Delta) = \tilde{\delta}(\Gamma_1,\Gamma_2,\Delta) \ . \tag{4.16c}$$

Thus $\tilde{\delta}(\Gamma_1,\Gamma_2,\Delta)$ is a positive even function of Δ and a symmetric function of Γ_1,Γ_2 with unit area under its graph. Since its magnitude is determined by the overlapping of the two f functions in (4.15), it has the analogous bell-shape dependence on Δ with a typical width of about $\Gamma_1+\Gamma_2$. In the limit $\Gamma_1,\Gamma_2 \to 0$ it turns into the usual δ function $\delta(\Delta)$.

Combining Eqs. (4.10), (4.14), and (4.15), the mean-squared matrix element of the density matrix operator is obtained:

$$\overline{|\rho_{\alpha\beta}^{(21)}|^2} = D_1\, \tilde{\delta}(\Gamma_1,\Gamma_2,\Delta)\, \langle n_\alpha(1-n_\beta)\rangle_2 \ , \tag{4.17a}$$

where $\Delta = E^{(2)} - E^{(1)} - \omega_{\alpha\beta}$. Starting from the same equation (4.8) one may arrive at a different form of the answer if the summation over the complete set of $|j\rangle$ instead of $|i\rangle$ in (4.9) is performed:

$$\overline{|\rho_{\alpha\beta}^{(21)}|^2} = D_2\, \tilde{\delta}(\Gamma_1,\Gamma_2,\Delta)\, \langle n_\beta(1-n_\alpha)\rangle_1 \ , \tag{4.17b}$$

where the symmetry properties (4.16) have been used. These formulas have been obtained in [19–21] given that the Lorenzian approximation is used for $\overline{C_j^2}$. Based on a simple model [3] the Lorenzian approximation allows one to check that in the perturbation theory regime, when the transition between distant components is studied ($|E^{(2)}-E^{(1)}+\omega_{\beta_\alpha}| \gg \Gamma_{1,2}$, and $\Gamma_1 \sim \Gamma_2$ is assumed), the answer is given by half of the sum of (4.17a) and (4.17b) [19,21].

Assuming the Lorenzian and the squared Lorenzian forms of $f(\epsilon)$, one respectively obtains the following two expressions for $\tilde{\delta}(\Gamma_1,\Gamma_2,\Delta)$:

$$\tilde{\delta}(\Gamma_1,\Gamma_2,\Delta) = \begin{cases} \frac{1}{2\pi}\,\frac{\Gamma_1+\Gamma_2}{\Delta^2+(\Gamma_1+\Gamma_2)^2/4} & \text{(Lorenzian)} \\ \frac{1}{4\pi}\,\frac{(\Gamma_1+\Gamma_2)\left[\Gamma_1\Gamma_2(\Gamma_1+\Gamma_2)^2+[\Delta^2+(\Gamma_1+\Gamma_2)^2/4](\Gamma_1^2+\Gamma_2^2-\Gamma_1\Gamma_2)\right]}{[\Delta^2+(\Gamma_1+\Gamma_2)^2/4]^3} & \text{(squared Lorenzian).} \end{cases} \tag{4.18}$$

The physics beyond Eqs. (4.17) is quite transparent. Suppose the spread widths of the compound states are of the same order of magnitude $\Gamma_1 \sim \Gamma_2 \sim \Gamma$ and the energy interval is not large: $|\Delta| < \Gamma$. Then $\tilde{\delta} \sim \Gamma^{-1}$, and since the number of principal components is $N \sim \Gamma/D$, the mean-square matrix element is $\overline{|\rho_{\alpha\beta}^{(21)}|^2} \sim N^{-1}\langle n_\beta(1-n_\alpha)\rangle_1$ [we used Eq. (4.17b) here]. The N^{-1} factor is a natural consequence of the fact that the compound states are chaotically distributed over about N simple basis states. The second factor shows that the contribution of the $\beta \to \alpha$ single-electron transition to the matrix element between the compound states $|1\rangle$ and $|2\rangle$ is proportional to the joint probability for the β state to be occupied and the α state to be vacant in the initial state $|1\rangle$ [or vice versa, in the final state $|2\rangle$, if one considers Eq. (4.17a)]. When the $\omega_{\alpha\beta}$ energy becomes noticeably different from $E^{(2)}-E^{(1)}$ ($|\Delta| > \Gamma$) the mean-squared $\rho_{\alpha\beta}^{(21)}$ drops down due to the decrease of the probability to find configurations differing by the state of only one electron (β vs α) among the principal components of the $|1\rangle$ and $|2\rangle$ compound states, respectively. This slump is described by the spread δ function $\tilde{\delta}$. Therefore, the presence of $\tilde{\delta}$ in (4.17) is a specific manifestation of the energy conservation for the transitions between the chaotic state components with finite widths Γ.

In order that both formulas (4.17) give the same results a fulfillment of the following condition is required:

$$D_1\langle n_\alpha(1-n_\beta)\rangle_2 = D_2\langle n_\beta(1-n_\alpha)\rangle_1 \ . \tag{4.19}$$

Here we present a qualitative argument in favor of that. Suppose all occupancies are small: $n_\alpha, n_\beta \ll 1$, i.e., the number of single-electron states is much larger than the number of electrons involved. Then $\langle n_\alpha(1-n_\beta)\rangle_2 \simeq \langle n_\alpha\rangle_2$ and $\langle n_\beta(1-n_\alpha)\rangle_1 \simeq \langle n_\beta\rangle_1$. If the occupancy of, say, the α state in $|2\rangle$ is smaller than that of the β state in $|1\rangle$: $\langle n_\alpha\rangle_2 < \langle n_\beta\rangle_1$, then it means that there are more single-particle states available within the compound state $|2\rangle$ than within $|1\rangle$. But having more single-particle states available, the density of many-electron states in the vicinity of $|2\rangle$ is larger and the corresponding level spacing is smaller: $D_2 < D_1$. The latter balances the difference in the occupancies in (4.19).

In the present paper the basis of states Ψ_{Ji} (2.4) with certain total angular momentum and parity is used. The statistical independence of the components C_i expressed by (4.3) and (4.5) follows then from the large magnitude of the residual interaction, which mixes the components of the eigenstates in a nearly random fashion (Sec. III). This mixing takes place not only among the principal components within the energy band of the spread width Γ, but also among the smaller "distant" components. In contrast with that, the mixing of the single-determinant basis states Ψ_i (2.3) may never be considered as com-

plete, as long as the exact quantum number of the total angular momentum exists (i.e., while the Hamiltonian commutes with the corresponding operator $\hat{J}^2$). On the other hand, the mixing of the single-determinant states takes place irrespectively of the magnitude of the residual interaction because the eigenstates of the Hamiltonian are necessarily the eigenstates of the $\hat{J}^2$ operator. This fact alone introduces a kind of randomness into the C_i components due to the quasichaotic behavior of the coefficients of the angular momentum addition (e.g., the Clebsch-Gordan coefficients, in the simplest case). Despite this "angular" contribution to chaos, rigorously speaking, the use of the Ψ_{Ji} basis looks more consistent if one aims to investigate the true chaotic properties of the eigenstates. This is the approach we adopted performing the numerical investigation of the Ce compound states in Sec. III. Below we consider the modifications it required to derive the Eqs. (4.17) for the mean-squared matrix element. Henceforth we assume that the basis states $|i\rangle, |j\rangle$ in (4.8) are the states with definite angular momentum J and its projection M. Accordingly, the average level spacing D, the number of principal components N, and the spread width Γ are understood in the same way as in Sec. III, i.e., in reference to a particular J^π manifold. For the sake of simplicity the transition matrix element between the states $|1\rangle$ and $|2\rangle$ of the same angular momentum J will be considered.

In order to retain the validity of the closure used to obtain Eq. (4.9) from Eq. (4.8), one must be sure that the action of the operator [$\hat{M}^\dagger$ in (4.4) or $a^\dagger_\beta a_\alpha$ in (4.8)] onto the $|j\rangle$ state in the matrix element $\langle i|\cdots|j\rangle$ does not take this state out of the subspace of the $\langle i|$ states. We will ensure that by considering the matrix element of a scalar or a pseudoscalar operator. It can be expressed in terms of the reduced density matrix operator of the zero rank $\hat{\rho}^0_{nlj,n'l'j}$ [Appendix C, Eq. (C6), $J_1 \equiv J$]:

$$\hat{\rho}^0_{nlj,n'l'j} = \left(\frac{2J+1}{2j+1}\right)^{1/2} \sum_m \hat{\rho}_{nljm,n'l'jm} = \left(\frac{2J+1}{2j+1}\right)^{1/2} \sum_m a^\dagger_{nljm} a_{n'l'jm} \,. \tag{4.20}$$

Note that its diagonal value ($nl = n'l'$) is proportional to the operator $\hat{n}_{nlj}$ of the number of electrons in the subshell nlj: $\hat{\rho}^0_{nlj,nlj} = \left(\frac{2J+1}{2j+1}\right)^{1/2} \sum_m a^\dagger_{nljm} a_{nljm} \equiv \left(\frac{2J+1}{2j+1}\right)^{1/2} \hat{n}_{nlj}$.

Introducing the operator (4.20) into (4.4) and following the steps outlined by Eqs. (4.8), (4.9), etc., the mean-squared matrix element of the zero rank reduced density matrix operator (4.20) is obtained in the form similar to (4.17):

$$\overline{\left(\rho^{(21)0}_{nlj,n'l'j}\right)^2} = \begin{cases} D_1\, \tilde{\delta}(\Gamma_1,\Gamma_2,\Delta) \left(\frac{2J+1}{2j+1}\right) \langle n_{nlj}(1-\frac{n_{n'l'j}}{2j+1})\rangle_2 & \text{(4.21a)} \\ D_2\, \tilde{\delta}(\Gamma_1,\Gamma_2,\Delta) \left(\frac{2J+1}{2j+1}\right) \langle n_{n'l'j}(1-\frac{n_{nlj}}{2j+1})\rangle_1 & \text{(4.21b)} \end{cases}$$

where $\Delta = E^{(2)} - E^{(1)} + \omega_{n'l'j,nlj}$. In deriving this formula an additional assumption has been made that the occupancies of the $nljm$ and $n'l'jm$ states are statistically independent and the states with different m within the same nlj shell are equally populated. This seems quite plausible for a system with several electrons in the valence shells. Moreover, this supposition influences only the "emptiness" factors $(1-\frac{n_{nlj}}{2j+1})$ in (4.21a) and (4.21b) that are at any rate close to 1 when the number of single-electron states available is much greater than the number of electrons involved.

B. Numerical calculations vs the statistical theoretical approach

In this section the results of the calculation of the matrix elements between the chaotic states are presented. The question behind these calculations, as well as behind the study of the chaotic states as a whole, is the existence of the dynamical enhancement of small perturbations in systems with chaotic spectra. Forestalling the calculations, we would like to claim that this enhancement is indeed observed in the spectrum of the Ce atom.

As an example of a small perturbation one may consider the parity-violating weak interaction or the interaction induced by the electron dipole moment, which violates both parity and time invariance (see, e.g., [22]). The latter interaction has an especially simple structure. Being a pseudoscalar it violates parity but conserves angular momentum. Hence its matrix elements are expressed in terms of the reduced density operator of the zeroth rank (see Appendix C). We will have this particular example in mind when performing the calculations.

The matrix elements $\rho^{(ik)0}_{nlj,n'l'j}$ of the reduced density matrix operator of the zeroth rank [Eq. (C6)] have been calculated between the first 140 odd (i) and even (k) states of $J = 4$. For the given basis of single-electron orbitals the selection rules allow the following six transitions $nlj - n'l'j$: $6s_{1/2}-6p_{1/2}$, $5d_{5/2}-4f_{5/2}$, $6p_{3/2}-5d_{3/2}$, and the reverse ones. The mean-squared values of the matrix elements $\overline{\left(\rho^{(ik)0}_{nlj,n'l'j}\right)^2}$ have been obtained for the $i,k = 10,20,\ldots,130$ levels using the averaging over a square window $i \pm 9, k \pm 9$ (the window size is $W = 19$).

In accordance with the random Gaussian-like distribution of $\rho^{(ik)0}_{nlj,n'l'j}$ (see below) the numerically obtained mean values of the matrix elements proved to be small: $\overline{\rho^{(ik)0}_{nlj,n'l'j}} \sim \left[\overline{\left(\rho^{(ik)0}_{nlj,n'l'j}\right)^2}\right]^{1/2}/W$ and displayed stochastic

variations with i and k. However, the dependence of the mean-*squared* matrix elements on the cardinal numbers of the eigenstates looks regular and relatively smooth. As an example, the root mean square of $\rho^{(ik)0}_{6s_{1/2}6p_{1/2}}$ is presented in Fig. 16(a). [Henceforth, and in Fig. 16 as well, an additional factor of $\left(\frac{2j+1}{2J+1}\right)^{1/2}$ is used when calculating the matrix elements and the corresponding operator is $\left(\frac{2j+1}{2J+1}\right)^{1/2}\hat{\rho}^0_{nlj,n'l'j} = \sum_m a^\dagger_{nljm}a_{n'l'jm}$. The use of this operator instead of (4.20) under the same name of the reduced density matrix of the zeroth rank should not bring any confusion.]

One can easily explain the observed behavior of $\left[\overline{\left(\rho^{(ik)0}_{6s_{1/2}6p_{1/2}}\right)^2}\right]^{1/2}$. It follows from the average energies of the configurations (Table I) that the energy $\omega_{6p_{1/2}6s_{1/2}}$ of the single-electron transition $6s_{1/2} - 6p_{1/2}$ is about 2 eV. Consequently, this single-electron transition is favored if the even state k is approximately 2 eV higher than the odd state i: a feature described in Eqs. (4.17) and (4.21a) and (4.21b) by the spread δ function $\tilde{\delta}(\Gamma_k, \Gamma_i, E^{(k)} - E^{(i)} - \omega_{6p_{1/2}6s_{1/2}})$. Therefore, the even state numbers k for the favorable transitions (large $\left[\overline{\left(\rho^{(ik)0}_{6s_{1/2}6p_{1/2}}\right)^2}\right]^{1/2}$ values) are noticeably larger than the corresponding odd level numbers i. In turn, the decline of the surface in Fig. 16(a) towards higher odd levels is connected with the decrease of the occupancy of the $6s_{1/2}$ orbital (Fig. 6), and this fact is taken into account by the average occupancy factors in Eqs. (4.17) and (4.21a) and (4.21b). Thus it is quite natural that the values of the mean-root-squared matrix element obtained by means of Eqs. (4.21a) and (4.21b) demonstrate the same behavior [Fig. 16(b)].

Having calculated the root-mean-squared matrix elements, one can easily check the statistics of the matrix elements by normalizing them in the following way: $\rho^{(ik)0}_{6s_{1/2}6p_{1/2}}/\sigma^{(ik)}$, where $\sigma^{(ik)} \equiv \left[\overline{\left(\rho^{(ik)0}_{6s_{1/2}6p_{1/2}}\right)^2}\right]^{1/2}$ is the local root mean square of the matrix element. Thus the systematic dependence of the magnitude of the matrix element on i and k is eliminated. A histogram describing the distribution of the 3136 normalized matrix elements for $i, k = 80 - 135$ is compared in Fig. 17 with the Gaussian distribution with zero mean and unit variance. There is a characteristic difference between the histogram and the curve: the former shows greater numbers of both small and large values of the variable. The descrepancy observed is larger for the matrix elements between lower levels, especially if the latter belong to the odd manifold. We believe that this feature is a manifestation of incomplete mixing of the basis states by the residual interaction within the spread width Γ. If, for instance, there were other quantum numbers besides the angular

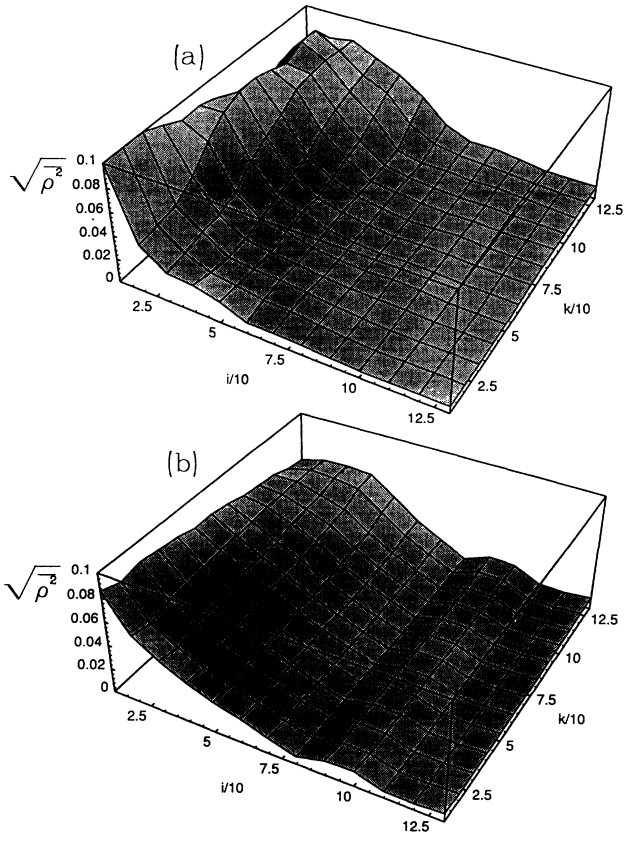

FIG. 16. Comparison of the numerical calculation of the matrix elements between the chaotic states with the results of the statistical theoretical approach. Shown is the dependence of the root-mean-squared matrix elements of the reduced density matrix operator $\left[\frac{2j+1}{2J+1}\overline{\left(\rho^{(ik)0}_{6s_{1/2}6p_{1/2}}\right)^2}\right]^{1/2}$ ($j = 1/2$, $J = 4$) on the ordinal numbers of the odd (i) and even (k) levels. (a) Window-averaged matrix elements from the CI calculations and (b) obtained from Eq. (4.21a).

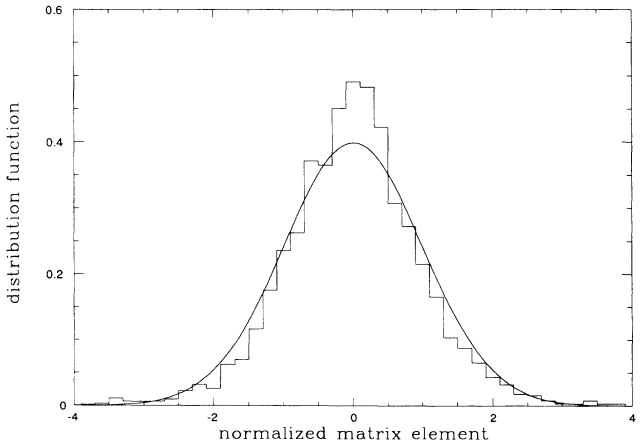

FIG. 17. The distribution of the normalized matrix element of the reduced density matrix operator $\rho^{(ik)0}_{6s_{1/2}6p_{1/2}}\left[\overline{\left(\rho^{(ik)0}_{6s_{1/2}6p_{1/2}}\right)^2}\right]^{-1/2}$ for $i, k = 80 - 135$ levels (histogram) compared with the Gaussian distribution (solid curve).

momentum and parity, then some of the matrix elements might be exactly zero due to the corresponding selection rules (others being larger, since $\sum_k \langle i|\hat{M}|k\rangle\langle k|\hat{M}|i\rangle$ does not depend upon the "degree of chaos" among the k states). Figure 17 suggests that in our numerical example the states' mixing is nearly complete and there are only traces of the abolished selection rules in it (see also Appendix E where the statistics of the components are analyzed).

An extensive test of Eqs. (4.21a) and (4.21b) including four different single-electron transitions is presented in Fig. 18. It shows the cross sections of the surfaces analogous to those in Fig. 16 with $i = 80$ (odd) or $k = 80$ (even) fixed. As one can see, there is generally a good agreement between the matrix elements calculated with the true CI wave functions and those obtained using the statistical approach outlined in Sec. IV A. To calculate the latter from Eq. (4.21a) and (4.21b) we used the widths Γ and the numbers of principal components N presented in Figs. 14 and 15. The average occupancy factors $\langle n_{nlj}(1 - \frac{n_{n'l'j}}{2j+1})\rangle = \overline{n_{nlj}} - \frac{1}{2j+1}\overline{n_{nlj}n_{n'l'j}}$ were obtained in the same way as shown in Figs. 6 and 7. The second term (correlated product of the occupancies) is usually rather small and can be approximated as $\overline{n_{nlj}}\ \overline{n_{n'l'j}}$ (though we calculated it exactly).

The most problematic point when applying Eqs. (4.21a) and (4.21b) is to find the correct energies of the single-electron transitions $\omega_{nlj,n'l'j'}$. This is not simply a consequence of the complicated procedure used to obtain the basis of the single-electron orbitals in the present CI calculations (Sec. II C and Appendix B) and the absence of a simple single-electron Hamiltonian which might produce them. There is in fact a much deeper question: when we consider a pair of many-electron basis states which differ by the position of one electron [say, one of the states is $\ldots (nlj)^{q_1}(n'l'j')^{q_2}\ldots$ and the other one is $\ldots (nlj)^{q_1+1}(n'l'j')^{q_2-1}\ldots$], is it true that the energy difference between these states is a well defined quantity? In other words, can its magnitude be given irrespectively of the occupancies of other orbitals, as well as of q_1 and q_2? Formulating this question we have in mind that in accordance with Sec. III B the energy positions of the many-electron basis states determine their mixing in the chaotic eigenstates.

The answer to the above question is not straightforward. The energies of the single-electron transitions demonstrate rather strong dependence on the "environment" in which the transitions take place. In Table IV we present the single-electron transition energies estimated using the average configuration energies from Table I. However, if the uncertainty in the value of $\omega_{nlj,n'l'j'}$ is less than the total width $\Gamma_1 + \Gamma_2$ of the function $\tilde{\delta}(\Gamma_1, \Gamma_2, \Delta)$,

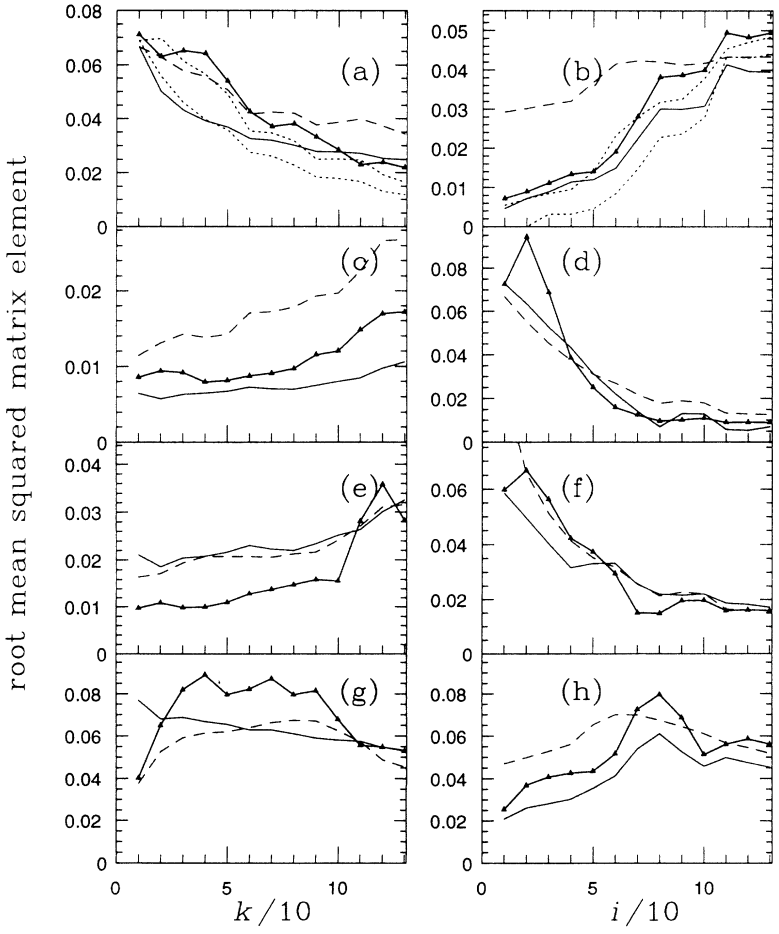

FIG. 18. The dependence of the root-mean-squared matrix elements of the reduced density matrix operator $\left[\frac{2j+1}{2J+1}\overline{\left(\rho^{(ik)0}_{nlj,n'l'j}\right)^2}\right]^{1/2}$ on the cardinal number of the even state k (left column, $i = 80$ is fixed) and on the cardinal number of the odd state i (right column, $k = 80$ is fixed). Shown are the window-averaged results of the CI calculations (solid triangles) and the results obtained from Eq. (4.21a) (solid line) and Eq. (4.21b) (dashed line), using the Lorenzian approximation for $w(E_j; E, N, \Gamma)$. The figures correspond to the following transitions $nlj - n'l'j$: (a) and (b) $6p_{1/2} - 6s_{1/2}$, (c) and (d) $6s_{1/2} - 6p_{1/2}$, (e) and (f) $5d_{5/2} - 4f_{5/2}$, (g) and (h) $4f_{5/2} - 5d_{5/2}$. In (a) and (b) the values from Eqs. (4.21a) and (4.21b) obtained for the squared Lorenzian shape of $w(E_j; E, N, \Gamma)$ are also shown (dotted lines).

TABLE IV. Energies of the single-electron transitions $nlj - n'l'j$ obtained from the differences between the average energies of the odd and even configurations.

nlj	$n'l'j$	Minimal $\Delta E_{\rm conf}$[a] (eV)	Maximal $\Delta E_{\rm conf}$[a] (eV)	$\omega_{nlj,n'l'j}$[b] (eV)
$6p_{1/2}$	$6s_{1/2}$	1.67	2.70	2.00
$6s_{1/2}$	$6p_{1/2}$	−2.74	−2.01	−2.00
$5d_{5/2}$	$4f_{5/2}$	−4.27	0.03	−2.7
$4f_{5/2}$	$5d_{5/2}$	−0.07	2.07	1.1

[a]Here we neglected the difference between the energies of different spin-orbital components $j = l \pm \frac{1}{2}$.
[b]These energies are used for the calculation of the root-mean-squared matrix elements of the density matrix operator in the statistical approach.

a fixed value of $\omega_{nlj,n'l'j'}$ can be used, and the difference between the real energy of the single-electron transition and the fixed value of $\omega_{nlj,n'l'j'}$ should not manifest too strongly. The values chosen for the calculation of $\left[\overline{\left(\rho^{(ik)0}_{nlj,n'l'j}\right)^2}\right]^{1/2}$ are shown in the last column of Table IV.

Returning to the results in Fig. 18 one may notice that in a number of cases the matrix elements obtained via the statistical approach reproduce quite subtle features of the curves from the CI calculations. This is conclusive proof of the validity of the statistical approach to the calculation of the mean-squared matrix element between chaotic states. There is also a reasonable overall agreement between the two ways of calculation: Eq. (4.21a) and Eq. (4.21b). There are also indications that a linear combination of the two formulas might often yield the best result (see the check of the perturbation theory limit in [21]).

If one assumes a stronger localization than that given by the Lorenzian shape of $w(E_j; E, N, \Gamma)$, the dependence of $\tilde{\delta}(\Gamma_1, \Gamma_2, \Delta)$ on energy Δ becomes more abrupt [Eq. (4.18)]. This is demonstrated in Figs. 18(a) and 18(b) for the squared Lorenzian approximation for $w(E_j; E, N, \Gamma)$. The average slope of the corresponding curves seems slightly closer to that of the CI calculated ones. Nevertheless, as the true behavior of the distant components is different from both the Lorenzian and the squared Lorenzian shapes of $w(E_j; E, N, \Gamma)$ (Appendix D), this question needs a more careful investigation. This would also require a consideration of transitions between the chaotic states lying further apart on the energy scale, so that large Δ could be probed.

V. DYNAMICAL ENCHANCEMENT OF SMALL PERTURBATIONS

Let us consider the admixture of the state $|i\rangle$ to the state $|k\rangle$ due to the effect of the perturbation $\hat{M}$. The magnitude of the admixture is given by

$$\eta = \left| \frac{\langle i|\hat{M}|k\rangle}{E^{(i)} - E^{(k)}} \right| . \tag{5.1}$$

In systems with dense spectra and chaotic eigenstates the matrix element in the numerator is reduced by a factor of $N^{-1/2}$ due to the randomness of the components' contributions. The denominator for closely lying states is about $D \sim N^{-1}\Gamma$. Thus an enhancement of the mixing coefficient (5.1) proportional to $N^{1/2}$ is expected with respect to the mixing in a system with a spectrum dominated by single-particle features. It will be shown below that this enhancement indeed exists in the chaotic spectrum of the Ce atom and the magnitude of the enhancement agrees with this simple estimate.

If one considers the mixing of states of different J^π manifolds, it is a reasonable assumption that the spacing between the closest levels $|E^{(i)} - E^{(k)}|$ obeys Poissonian statistics (there is no level repulsion effects). Assuming further that the numerator in Eq. (5.1) has a typical magnitude of M_0, one can obtain the distribution for the mixing coefficients η for the closest pairs of levels:

$$f(\eta) = \frac{\eta_0}{\eta^2} e^{-\eta_0/\eta} , \tag{5.2}$$

where $\eta_0 = M_0/D$ gives the typical magnitude of mixing and D is the average spacing between the closest levels of the different manifolds. If one attempts to find the expectation value for the mixing coefficient from Eq. (5.2), the result would be $\overline{\eta} = \infty$ since the corresponding integral diverges as $\int d\eta/\eta$. It does not only mean that very large values of η can be observed, but it also means that their number is large. The probability to observe a value of η larger than certain η_1 is $P(\eta > \eta_1) \simeq \eta_0/\eta_1$ (provided $\eta_1 \gg \eta_0$).

In order to check these considerations we have calculated the mixing coefficient between the 21–70 odd levels and the 1–140 even levels. In doing so we have chosen the mixing operator to be $\hat{M} = \left(\frac{2j+1}{2J+1}\right)^{1/2} \hat{\rho}^0_{6s_{1/2}6p_{1/2}}$ (its root-mean-squared matrix elements are shown in Fig. 16). For each of the 50 odd levels the 140 mixing coefficients η (5.1) were calculated, and we chose the largest of them. Usually it corresponded to the mixing of the closest even level with a given odd one. The distribution of the resulting 50 values of η is presented in Fig. 19. There it is fitted by the model distribution (5.2) with $\eta_0 = 1.15$ eV^{-1}. The results of the χ^2 tests support the validity of the fit. It is easy to check that the probability of finding a value of η greater than 10 eV^{-1} is about 10%. Remarkably, this is exactly the number of η values falling out of the range shown in Fig. 19.

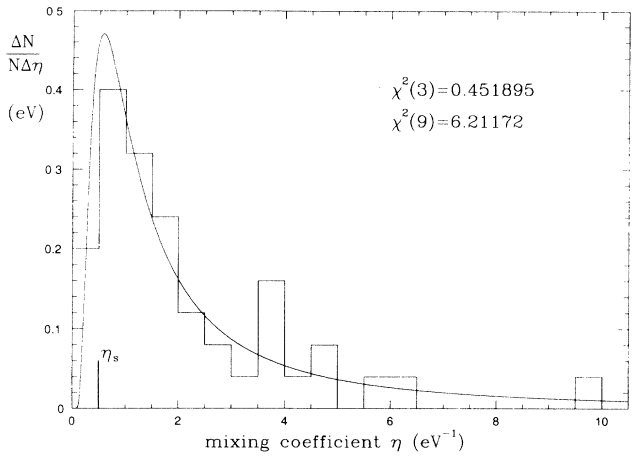

FIG. 19. The distribution function for the maximal mixing coefficient $\eta = \max_k \left\{ \left(\frac{2j+1}{2J+1}\right)^{1/2} \left| \rho^{(ik)0}_{6s_{1/2}6p_{1/2}} / (E^{(k)} - E^{(i)}) \right| \right\}$ ($k = 1-140$), for the 50 odd levels $i = 21-70$. The histogram is fitted by $f(\eta) = \eta_0 \eta^{-2} \exp(-\eta_0/\eta)$ with $\eta_0 = 1.15$. Also shown is the magnitide of the single-electron mixing $\eta_s = 0.5$ eV^{-1}. The results of the χ^2 tests are shown for the first four and ten bins. Five η values among 50 fall beyond $\eta = 10$: $\eta = 12.5, 20.4, 37.7, 41.8, 98.0$.

As mentioned above, the calculation of the mean mixing coefficient is meaningless. Its magnitude, strictly speaking infinite, would depend upon the subset of η chosen (the larger the subset, the greater the mean value). In our case $\overline{\eta} \simeq 6.1$ eV^{-1} is obtained, which is much greater than the typical mixing $\eta_0 = 1.15$ eV^{-1}. It is interesting to estimate the typical mixing one might expect in this situation. The average even level spacing at 2–4 eV is about $D \simeq 0.025$ eV. The typical root-mean-squared values of the matrix elements for 21–70 odd and even levels are about $M_0 = 0.03$ (Fig. 16). Taking into account the fact that the average spacing between a given odd level and the closest even one is $\frac{D}{2}$, one obtains a typical mixing of $\frac{2M_0}{D} \sim 2$ eV^{-1}. This rough estimate is in good agreement with the η_0 value obtained by fitting the histogram.

Despite the fact that the transition chosen is not the best for observing the dynamical enhancement (the domain of maximal matrix elements lies to the side of the $E^{(i)} \simeq E^{(k)}$ region), we can easily demonstrate its existence. Let us find out the magnitude of single-particle mixing η_s, which one might expect in a system with a sparse, "regular" spectrum, like that of the Cs atom. The energy difference between the $6s_{1/2}$ and $6p_{1/2}$ levels in Ce is $\omega_{6p_{1/2}6s_{1/2}} \simeq 2$ eV. Since the mixing matrix element of the $\left(\frac{2j+1}{2J+1}\right)^{1/2} \hat{\rho}^0_{6s_{1/2}6p_{1/2}}$ operator [see Eq. (4.20)] between the single-particle $6s_{1/2}$ and $6p_{1/2}$ states is equal to 1, the mixing coefficient is $\eta_s = 1/\omega_{6p_{1/2}6s_{1/2}} \simeq 0.5$ eV^{-1}. Thus we see that the characteristic mixing in Ce $\eta_0 = 1.15$ eV^{-1} is greater than η_s by a factor of 2.3, not to mention that some particular values of η exceed η_s by one or even two orders of magnitude. The statistical enhancement factor in our example (2.3) turned out to be smaller than the potential value of $\sqrt{N} \simeq 10$. This can be explained from Eqs. (4.21a) and (4.21b) since both $\hat{\delta}$ and the occupancy factor in it are approximately two times smaller than their maximal values.

VI. CONCLUSIONS

It has been shown in the paper that the excited states of the rare-earth atom Ce at excitation energies above 2 eV have chaotic structure. These states are similar to the compound resonances in heavy nuclei. They are formed as superpositions of large numbers of simple basis states. The mixing of the basis states is determined by the strength of the residual interaction and the level spacing of the spectrum. It takes place within a certain energy range, i.e., within their spread width. The localization of the squared components of the eigenstates considered as functions of the basis states' energies is described by the Lorenzian curve. Beyond the energy range of a few spread widths a stronger localization (enhanced exponential) has been observed, together with the selective mixing of distant components. The matrix elements between the chaotic states are calculated both directly and using the statistical approach. Within the latter they are expressed in terms of the parameters of the chaotic eigenstates, the average single-electron occupancies, and the energies of the single-electron transition. The validity of this approach is proved by direct comparison with the results of the numerical calculations. It is shown that a statistical enhancement of small perturbations takes place in the dense spectrum of chaotic levels. This favors the observation of a strong mixing of levels belonging to different J^π manifolds and large observable parity-nonconcerving and time-invariance violating effects in such systems.

In the paper we used chaotic properties of the compound eigenstates to calculate the matrix elements and the statistical enhancement factor. However, one can also try to formulate a criterion for the emergence of chaos in quantum system based on the enhancement of perturbations. The latter property is somewhat similar to the exponential divergence of trajectories due to the perturbation in the initial conditions in classical chaotic systems. Indeed, the enhancement of small perturbations (proportional to $\sqrt{N} \sim e^{\alpha n}$, where n is the number of "active" particles) means that any small variation of the Hamiltonian drastically changes the positions of energy levels and the weights of basis components in each compound state. We observed this phenomenon in the numerical calculations where the smallest changes in the basis single-electron orbitals (see Appendix B) or the introduction of screening coefficients in the Coulomb integrals noticeably changed the positions and the component constitution of the individual compound states. It is natural to suppose that in such a situation the compound states demonstrate chaotic properties.

In the Appendixes a comparison is presented of the results of the present paper with the predictions of the BRM models, and with some other approaches investigating quantum chaotic systems.

The authors believe that the physical picture obtained of the realistic quantum chaotic system — the spectrum of the Ce excited states—can give insight into other complex systems: actinide atoms, molecules, clusters, mesoscopic systems, compound nuclei, etc.

ACKNOWLEDGMENTS

The authors are deeply indebted to I. I. Tupizin for the permission to use his original Hartree-Fock-Dirac and configuration-interaction codes. They would like also to thank B. V. Chirikov for valuable discussions on the problems of the quantum chaos. M. G. K. is grateful to the Godfrey Fund and to the staff and colleagues at the School of Physics, University of New South Wales for their hospitality during his two month visit when the present work was started.

APPENDIX A: STATISTICS OF LEADING PERCENTAGES — THE GAUSSIAN MODEL

In the paper [8] a sequence of 35 $J^\pi = 1^+$ energy levels of Ce lying at energy of $E = 2 - 3$ eV ($D = 0.027$ eV) above the atomic ground state was considered. Though the results of the present work confirm the chaotic properties of Ce eigenstates, there are two important points which make the reliability of the numerical estimates of [8] questionable.

First, it was essential for the analysis of [8] that an assumption of the maximal quantum chaos was adopted. It included the supposition that the jth component C_j of the eigenstate obeys the Gaussian statistics, and the mean values are $\overline{C_j} = 0$ and $\overline{C_j^2} = N^{-1}$. However, in a real physical system perturbation mixes up an infinite number of basis states and there are many *small* components, besides a number of N *principal* ones. It makes the overall statistics of components different from the Gaussian statistics (see Appendix E). In particular, if one examines the leading components of the eigenstates, a normalization of $\overline{C_j^2} = FN^{-1}$ might be assumed, where $F = \sum_j C_j^2 < 1$, since the summation is performed over the principal components only.

Second, the key point of the numerical analysis of [8] was an expression for the mean maximal square $\overline{w_1}$ of N independent Gaussian variables x_j and that for the second largest square (w_2) as well. We argue that for large N the correct asymptotic formulas for $\overline{w_{1,2}}$ are $\overline{w_1} \sim 2\,\overline{x_j^2}\,\ln N$ and $\overline{w_2} \sim 2\,\overline{x_j^2}\,(\ln N - 1)$, which differ from those used in [8] by a factor of 2. The proof is given below.

Suppose x_j ($j = 1, 2, \ldots, N$) are independent Gaussian random variables with zero centroid and unit variance. The question is the following: what is the mean value of the maximal square $w_1(N)$ of them?

Introducing the squared variables $y = x^2$ and recalling that their probability density is $(2\pi y)^{-1/2}\exp(-y/2)$, one obtains

$$\overline{w_1(N)} \equiv N \int_0^\infty \frac{e^{-y/2}}{\sqrt{2\pi y}}\, y\, g^{N-1}(y)\, dy = \int_0^\infty y\, d(g^N(y))\,, \tag{A1}$$

where $g(y)$ is the probability that $x^2 < y$, and the factor N accounts for the fact that each of N squares x_j^2 may turn out to be the maximal one. An examination of the integrand in (A1) shows that it has a maximum around $y \sim 2\ln N$. Therefore, the asymptotic formula for $g(y)$ can be applied:

$$g(y) \equiv \int_0^y \frac{e^{-t/2}}{\sqrt{2\pi t}}\, dt \simeq 1 - 2\frac{e^{-y/2}}{\sqrt{2\pi y}} \simeq \exp\left(-\frac{2e^{-y/2}}{\sqrt{2\pi y}}\right) \quad (y \gg 1), \tag{A2}$$

where the last expression in (A2) is more convenient for calculating the Nth power of $g(y)$. Introducing a new variable $u = g^N(y)$ to calculate the integral (A1) (u runs from 0 to 1), one needs to express y in terms of u. It can be easily done by means of the asymptotic exponential expression (A2) for g:

$$y = 2\ln N - 2\ln(-\ln u) - \ln\frac{\pi y}{2}\,. \tag{A3}$$

Here the first item $2\ln N$ in the right hand side is the leading one. Hence it can be used for y in the third item. Calculating the integral $\int_0^1 y du$ and using [23] to integrate the second item in (A3), one obtains

$$\overline{w_1(N)} \simeq 2\ln N + 2\mathcal{C} - \ln(\pi \ln N)\,, \tag{A4}$$

where $\mathcal{C} \simeq 0.577$ is the Euler constant. Numerical evaluation of the integral (A1) shows that the asymptotic expression (A4) works with an amazing accuracy of better than 1% even for $N = 3$.

The mean value of the second large square of N independent Gaussian random variables is given by the integral below. It essentially involves the probability that $N - 2$ squared variables are less than y times the probability that one square is larger than y and a combinatorial $N(N-1)$ factor:

$$\overline{w_2(N)} = N(N-1)\int_0^\infty \frac{e^{-y/2}}{\sqrt{2\pi y}}\, y\, g^{N-2}(y)\,[1 - g(y)]\, dy\,. \tag{A5}$$

Reduced to a linear combination of $N\overline{w_1(N-1)} - (N-1)\overline{w_1(N)}$, (A5) can be easily estimated using the asymptotic expression (A4):

$$\overline{w_2(N)} \simeq \overline{w_1(N)} - 2 + (\ln N)^{-1} - N^{-1}\,. \tag{A6}$$

An account of both points mentioned above yields $F \simeq 0.6$ and $N \simeq 16$. Thus the estimated number of large components is in agreement with the one given in [8], though only 60% of the eigenstate normalization seems to be shared between them. The rest of the components are

smaller and their statistics cannot be probed by means of the leading percentages.

APPENDIX B: CI CALCULATIONS FOR CERIUM—CONSTRUCTION OF THE BASIS

The trial CI calculations we performed for Ce showed that the results (the energies and the configuration constitution of the eigenstates) are extremely sensitive to the way of calculating the single-electron orbitals. It was particularly noticeable for the $4f$ and $5d$ wave functions. Their radial behavior and the single-particle energies strongly depended on whether there were one or two electrons in the subshell during the self-consistent HFD calculation of the basis. Accordingly, different methods of calculating them favored (lowered the energies of) the configurations with one or two f or d electrons, respectively. Since we needed to calculate matrix elements between the many-electron states, it was important for us that all levels were calculated in the same basis. Finally, a balanced way to calculate that was found.

At the first stage the $4f$ wave functions were obtained in a self-consistent calculation of the $1s^2\cdots 5p_{1/2}^2 5p_{3/2}^4 4f^2 6s^2$ atomic state, which coincides with the configuration of the lowest $J^\pi = 4^+$ level. The core wave functions and the $4f$ ones were then "frozen" and the $6s^2 5d$ configuration (the lowest with $J^\pi = 4^-$) was calculated in the field of the $1s^2\cdots 4f$ residue, yielding the $6s$ and $5d$ orbitals. The $6p$ orbitals were calculated separately in the frozen field of the $1s^2\cdots 4f6s5d$, after the $1s^2\cdots 4f^2 6s5d$ state had been calculated in a self-consistent way. In doing the HFD calculations the Coulomb interaction between the electrons in the open subshells was averaged over the nonrelativistic configuration, using the statistical occupancies of the $j = l \pm \frac{1}{2}$ orbitals. The valence orbitals thus obtained were orthogonalized before being used in the CI calculations.

The resulting single-electron orbitals were used to construct single-determinant basis states (2.3) and the basis of states with definite J values (2.4). It is worth mentioning that none of the particular coupling schemes are used for the construction of the Ψ_{Ji} basis. Instead, the $\hat{J}^2$ eigenstates in the CI code [15] are generated for the states in each of the relativistic configurations with the help of the lowering operator $\hat{J}^-$. Starting from the single-determinant states with the maximal $\hat{J}_z$ projection and consequently applying the $\hat{J}^-$ operator and the orthogonalization procedure, the sets of the Ψ_{Ji} states with $J \geq M$ are obtained ($M = 4$). Each of the relativistic configurations chosen produces several states with $J = 4$ and some of them as much as 20 (the $4f_{5/2}4f_{7/2}5d_{5/2}6p_{3/2}$ odd and $4f_{5/2}4f_{7/2}5d_{3/2}5d_{5/2}$ even configurations). The numbers of Ψ_{Ji} states with $J = 4$, corresponding to each of the nonrelativistic configurations, are shown in Table I together with their average energies.

It might seem as a drawback of the approach used to construct the Ψ_{Ji} states that there is no reasonable way of classifying these states. However, in the case of the rare-earth spectrum large numbers of the states with fixed J are mixed together in a nearly random fashion, which makes doubtful the practical value of any coupling scheme.

APPENDIX C: REDUCED MATRIX ELEMENTS OF THE DENSITY MATRIX OPERATOR

The eigenstates calculated by the CI code have definite projections M of the total angular momentum. In order to calculate the M-independent values of the matrix elements it is convenient to express the answer in terms of the *reduced matrix elements* with the help of the Wigner-Eckhart theorem.

Suppose the states $|1\rangle \equiv |\Psi^{(1)}_{J_1 M_1}\rangle$ and $\langle 2| \equiv \langle \Psi^{(2)}_{J_2 M_2}|$ in (4.2) are the eigenstates of the $\hat{J}_z$ and $\hat{J}^2$ operators and $\hat{M}$ is an irreducible tensor operator of the Lth rank $\hat{M} \equiv \hat{T}^L_q$. According to the Wigner-Eckhart theorem

$$\langle 2|\hat{M}|1\rangle \equiv \langle \Psi^{(2)}_{J_2 M_2}|T^L_q|\Psi^{(1)}_{J_1 M_1}\rangle = (-1)^{J_2 - M_2} \begin{pmatrix} J_2 & L & J_1 \\ -M_2 & q & M_1 \end{pmatrix} \langle \Psi^{(2)}_{J_2} \parallel \hat{T}^L \parallel \Psi^{(1)}_{J_1}\rangle, \tag{C1}$$

where $\langle \parallel \parallel \rangle$ is the reduced matrix element. On the other hand, we can express the matrix element (C1) in terms of the transition matrix according to (4.6) and using the single-electron basis of $\alpha = nljm$ ($\hat{\rho}_{\alpha\beta} \to \hat{\rho}_{nljm,n'j'l'm'} = a^\dagger_{nljm} a_{n'l'j'm'}$):

$$\langle \Psi^{(2)}_{J_2 M_2}|T^L_q|\Psi^{(1)}_{J_1 M_1}\rangle = \sum_{\substack{nljm \\ n'l'j'm'}} \langle nljm|\hat{t}^L_q|n'l'j'm'\rangle \, \rho^{(21)}_{nljm,n'l'j'm'} \tag{C2}$$

$$= \sum_{\substack{nljm \\ n'l'j'm'}} (-1)^{j-m} \begin{pmatrix} j & L & j' \\ -m & q & m' \end{pmatrix} \langle nlj \parallel \hat{t}^L \parallel n'l'j'\rangle \times \rho^{(21)}_{nljm,n'l'j'm'} \, . \tag{C3}$$

Now we define the Lth rank reduced matrix element of the density matrix operator $\rho^{(21)L}_{nlj,n'l'j'}$ from the equation which connects the reduced matrix elements between the many-electron states with those between the single-electron states:

$$\langle \Psi^{(2)}_{J_2} \parallel \hat{T}^L \parallel \Psi^{(1)}_{J_1}\rangle = \sum_{\substack{nlj \\ n'l'j'}} \langle nlj \parallel \hat{t}^L \parallel n'l'j'\rangle \, \rho^{(21)L}_{nlj,n'l'j'} \, , \tag{C4}$$

where the summation runs over the single-electron orbitals $nlj, n'l'j'$ in contrast to (4.6) and (C2), where it involves the single-electron states, i.e., the summation over the angular momentum projections as well. It follows then from (C3) and (C4) that

$$\rho^{(21)L}_{nlj,n'l'j'} = (-1)^{J_2-M_2} \begin{pmatrix} J_2 & L & J_1 \\ -M_2 & q & M_1 \end{pmatrix}^{-1} \times \sum_{mm'} (-1)^{j-m} \begin{pmatrix} j & L & j' \\ -m & q & m' \end{pmatrix} \rho^{(21)}_{nljm,n'l'j'm'} \cdot \tag{C5}$$

This quantity is independent of any angular momentum projections involved (either $M_{1,2}$, or q, or m, m'). Formula (C5) was used in the numerical calculations to obtain the reduced matrix elements of the density matrix operator from the CI wave functions which are calculated at fixed values of the total angular momentum projections. Equation (C5) looks especially simple for $L = 0$ (consequently, $J_2 = J_1$, $j' = j$ and $m' = m$):

$$\rho^{(21)0}_{nlj,n'l'j} = \left(\frac{2J_1+1}{2j+1}\right)^{1/2} \sum_m \rho^{(21)}_{nljm,n'l'jm} \cdot \tag{C6}$$

The matrix element of the reduced diagonal ($n'l'j' = nlj$) density matrix operator of the zeroth rank between the identical states $|2\rangle = |1\rangle$ is given by

$$\rho^{(11)0}_{nlj,nlj} = \left(\frac{2J_1+1}{2j+1}\right)^{1/2} \sum_m \rho^{(11)}_{nljm,nljm} \cdot \tag{C7}$$

The sum on the right hand side yields the number of electrons in the nlj subshell. Thus the occupancy n_{nlj} of the nlj orbital in the state $|1\rangle$ is given by $n_{nlj} = \left(\frac{2j+1}{2J_1+1}\right)^{1/2} \rho^{(11)0}_{nlj,nlj}$.

APPENDIX D: LOCALIZATION PROPERTIES OF THE CHAOTIC STATES—DISTANT COMPONENTS

In this appendix we use perturbation theory to derive the equation governing the behavior of distant components of the BRM eigenstates and to obtain its asymptotic solution (3.6).

Suppose we calculate the eigenfunctions for the following infinite matrix H_{ij}:

$$H_{ij} = E_i\delta_{ij} + V_{ij}(1-\delta_{ij}) \quad (|i-j| \le b) \,, \tag{D1}$$

$$H_{ij} = 0 \quad (|i-j| > b); \quad (i,j = \ldots,-2,-1,0,1,2,\ldots) \,, \tag{D2}$$

where $E_i = iD$ are the diagonal energies with D spacing, b is the bandwidth, and V_{ij} are random variables with zero centroid and fixed variance: $\overline{V_{ij}} = 0$ and $\overline{V_{ij}^2} = V^2$. If one uses perturbation theory to obtain the eigenfunctions ψ_i of H_{ij} in terms of the eigenfunction $\psi_j^{(0)}$ of the $H_{ij}^{(0)} = E_i\delta_{ij}$ matrix, $\psi_i = \psi_i^{(0)} + \sum_j C_{ij}\psi_j^{(0)}$, the admixture of the state j to the i is given by

$$C_{ij} = \frac{V_{ji}\Pi_{ij}}{E_i - E_j} + \sum_k \frac{V_{jk}V_{ki}\Pi_{jk}\Pi_{ki}}{(E_i-E_j)(E_i-E_k)} + \sum_{km} \frac{V_{jk}V_{km}V_{mi}\Pi_{jk}\Pi_{km}\Pi_{mi}}{(E_i-E_j)(E_i-E_k)(E_i-E_m)} + \cdots \,, \tag{D3}$$

where $j,k,m,\ldots \ne i$ and Π_{ji} allows for the band structure of the matrix:

$$\Pi_{ji} = \begin{cases} 1, & |i-j| \le b \\ 0, & |i-j| > b. \end{cases} \tag{D4}$$

In writing Eq. (D3) we do not preserve the normalization of the ψ_i state and we do neglect the terms which have the same order in $V/\Delta E$ but a lower order of summation. The latter is based on an assumption that the bandwidth is large $b \gg 1$. This approximation is analogous to that made in [11].

Equation (D3) reveals an inherent feature of the band matrices. If one examines the mixing of distant components $|i-j| > b$, the lowest order $n = \left[\frac{|i-j|}{b}\right] + 1$ exists, below which the perturbation series items do not contribute to C_{ij}. Each of the numerators in Eq. (D3) contains a product $\Pi_{jk}\cdots\Pi_{mi}$, which determines a sequence of subscripts leading from the i state to the j state. The higher the order of the term, the larger the number of such sequences. Therefore, higher-order terms have greater statistical weight (though they may be suppressed by a greater power of $\frac{V}{\Delta E}$). It makes the mixing of distant components for the band matrix a nonperturbative problem in the sense that a certain number of items of the series (D3) yield comparable contributions to C_{ij} for given i and j.

If one averages C_{ij} over the ensemble of random matrices (D1) and (D2), one obtains $\overline{C_{ij}} = 0$ due to the statistical properties of the off-diagonal matrix elements. However, averaging C_{ij}^2, one obtains

$$\overline{C_{ij}^2} = \frac{V^2\Pi_{ji}}{(E_j-E_i)^2} + \sum_k \frac{V^4\Pi_{jk}\Pi_{ki}}{(E_k-E_i)^2(E_j-E_i)^2} + \sum_{km} \frac{V^6\Pi_{jk}\Pi_{km}\Pi_{mi}}{(E_k-E_i)^2(E_j-E_i)^2(E_m-E_i)^2} + \cdots \,, \tag{D5}$$

where all odd-power terms vanish due to the random nature of V_{ij} and we omit the terms which have less summations within each order. Introducing the notation $w(j-i) \equiv \overline{C_{ij}^2}$, valid since C_{ij} depends only on the "distance" between the states, one obtains from Eq. (D5) the following equation for w:

$$w(j-i) = \frac{V^2}{D^2}\,\frac{\Pi_{ji}}{(j-i)^2} + \frac{V^2}{D^2}\,\frac{1}{(j-i)^2}\,\sum_k \Pi_{jk}w(k-i) \,. \tag{D6}$$

If $|i-j| > b$ this equation turns into a homogeneous one:

$$w(j-i) = \frac{V^2}{D^2}\,\frac{1}{(j-i)^2}\,\sum_k \Pi_{jk}w(k-i) \,. \tag{D7}$$

If $w(k-i)$ is a smooth function of k (it is true for $b \gg 1$ since b fixes the typical variation scale for w), one can replace the sum in Eq. (D7) with an integral $\int_{j-b}^{j+b} w(k-i)dk$. Introducing a new variable $\xi \equiv \frac{j-i}{b}$ and a new function $\rho_w(\xi) \equiv w(\xi b)$ one obtains an integral equation

$$\rho_w(\xi) = \frac{q}{\xi^2}\int_{\xi-1}^{\xi+1}\rho_w(\xi')d\xi' \ , \qquad \text{(D8)}$$

where $q = \frac{V^2}{D^2 b}$. This equation exactly coincides with what one obtains from Eq. (35) of [11] for the asymptotic behavior of the strength function. Apparently, Eq. (D3) is valid only in the perturbation theory regime $\frac{V}{D} < 1$. Otherwise it cannot be used for calculating large components proximate to the eigenstate. However, if one applies it to distant components it leads to Eq. (D8), which holds irrespectively of the magnitude of the perturbation.

Before solving Eq. (D8) it is worthwhile to guess the answer by considering the series (D5). One may conjecture that for $E_j - E_i = Db\xi > 0$ the main contribution to $\overline{C_{ij}^2}$ and, consequently, to $\rho_w(\xi)$ comes from the nth order term of the series, where $n \simeq \xi$. This can be estimated as

$$t(\xi)\ \frac{V^{2n}}{(Db)^2(2Db)^2\cdots(nDb)^2} \sim t(\xi)\ \frac{1}{(\xi!)^2}\ \left(\frac{V}{Db}\right)^{2\xi} \ ,$$

where $t(\xi)$ takes into account the number of items in the sum which contribute to the nth order term. Using $\xi! \simeq \sqrt{2\pi\xi}\left(\frac{\xi}{e}\right)^{\xi}$ one obtains

$$\rho_w(\xi) \propto \frac{t(\xi)}{\sqrt{2\pi\xi}}\ \exp\left\{-2\xi\ln\left(\frac{\xi}{e}\ \frac{Db}{V}\right)\right\} \ . \qquad \text{(D9)}$$

The factor before the exponent is a slowly varying function of ξ and the main dependence of $\rho_w(\xi)$ on ξ is grasped by the exponent.

Therefore, in order to solve Eq. (D8) it is convenient to introduce a new function $y(\xi)$: $\rho_w(\xi) \equiv e^{y(\xi)}$. Supposing that $y(\xi)$ varies slowly on the scale of a bandwidth one may expand it in the integrand on the right hand side of Eq. (D8) as $y(\xi') = y(\xi) + y'(\xi)(\xi' - \xi)$ [note that $y'(\xi) < 0$, as $\rho_w(\xi)$ is decreasing at $\xi > 0$]. An equation then follows for $y'(\xi)$:

$$\frac{\sinh y'(\xi)}{y'(\xi)} = \frac{\xi^2}{2q} \ .$$

For $\xi^2 \gg q$ one may subsitute $\sinh y'(\xi) \simeq \frac{1}{2}e^{-y'(\xi)}$ and the following asymptotic solution is obtained:

$$y'(\xi) = -\ln\frac{\xi^2}{q} - \ln\left(\ln\frac{\xi^2}{q}\right) + \cdots \ .$$

It yields

$$\rho_w(\xi) = \text{const} \times \exp\left\{-2\xi\ln\left(\xi e^{-1}\sqrt{2q^{-1}\ln[\xi/\sqrt{q}]}\right)\right\}$$

$$(\xi > 0), \qquad \text{(D10)}$$

where the terms varying slower than ξ have been omitted from the exponent. This result confirms the perturbation theory estimate (D9). Since ρ_w is symmetric, it is sufficient to introduce $|\xi|$ instead of ξ to make Eq. (D10) valid for both positive and negative values of the argument. This solution corrects the erroneous one given in [11]. The magnitude of the constant in Eq. (D10) is determined by the normalization condition of the eigenstate and is, very roughly, inversely proportional to the number of principal components N^{-1}. The condition $\xi^2 \gg q$ of the validity of Eq. (D10) rewritten in terms of the energies and parameters of the matrix looks as follows: $|E_j - E_i| \gg b^{1/2}V$.

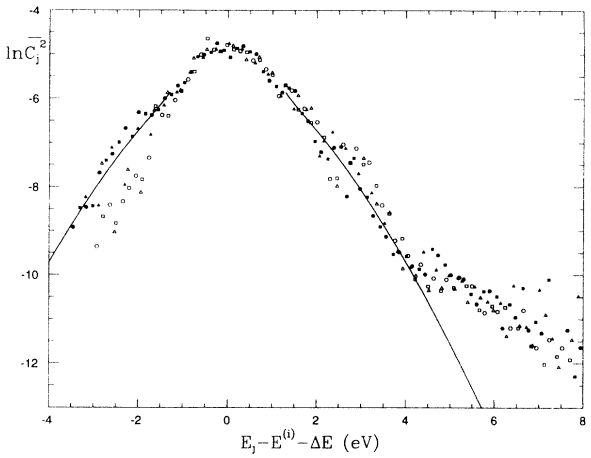

FIG. 20. The behavior of the distant components of the chaotic even eigenstates of Ce. The window-averaged $\overline{C_j^2}$ values are shown for the even levels: 60 (open triangles), 70 (open squares), 80 (open hexagons), 90 (solid triangles), 100 (solid squares), and 110 (solid hexagons). The solid curve shows the asymptotic behavior given by Eq. (3.6) (D10) with $V = 0.114$ eV, $D = 0.032$ eV, and $b = 80$ ($q = 0.16$).

In Fig. 20 we check the capacity of Eq. (D10) to describe the behavior of the distant components of the Ce $J^\pi = 4^+$ eigenstates. The states chosen have close numbers of principal components $N \simeq 120$ and widths $\Gamma \simeq 1.8$ eV (see Fig. 15). Hence the dependence of the numerically obtained $\overline{C_j^2}$ on the distance between the basis state energy E_j and the eigenvalue E (corrected by the ΔE shift) is essentially the same for them. In order to apply Eq. (D10) we used fixed values of the parameters from Sec. III A and Table II. Good agreement is observed between the numerical values and the asymptotic formula outside the 2 eV range around the maximum. The exception is a prominent high-energy shoulder on the numerical $\overline{C_j^2}$ due to the selective mixing of configurations.

APPENDIX E: THE ENERGY BANDWIDTH, THE ENTROPY LOCALIZATION LENGTH, AND THE DISTRIBUTION OF EIGENSTATES' COMPONENTS

In this appendix we check the applicability of approaches adopted for investigating BRM in model calculations to the system in consideration: the CI matrix and the chaotic eigenstates in Ce.

It has been pointed out in Sec. III A that the matrix elements H_{ij} exhibit a trend to group along the main diagonal, thus imposing a bandlike structure to the con-

figuration interaction matrix. In order to check it the mean-squared energy bandwidths [17] are calculated:

$$(\Delta E_i)^2 \equiv \frac{\sum_j (H_{ii} - H_{jj})^2 |H_{ij}|^2}{\sum_{j \neq i} |H_{ij}|^2} . \quad \text{(E1)}$$

The values of ΔE_i are presented in Fig. 21. Apart from the level-to-level fluctuations their dependence on i is on the whole amazingly flat. The average values of $\Delta E_i \simeq 1.9$ eV and $\Delta E_i \simeq 1.5$ eV characterize the energy bandwidths for the CI matrix for the odd and even $J = 4$ states, respectively. Using the average H_{ii} spacing of ~ 0.03 eV for both cases, estimates for the bandwidth b are obtained: $b \simeq 60$ (odd) and $b \simeq 50$ (even). Since the local spacing between the diagonal energies H_{ii} strongly varies along i, the local values of the bandwidth may be different from those given above. Thus, between the 30th and 150th even levels the average spacing of $D \simeq 0.014$ eV and $\Delta E_i \simeq 1.3$ eV produces $b \simeq 90$. This value is close to that used in Appendix D when studying the asymptotic behavior of the distant components.

As we have seen in Appendix D the asymptotic behavior of the distant components for the BRM with the leading diagonal, as well as for our numerical model, is different from the simple anzatz $|C_j^{(i)}| \propto \exp\left(-\frac{|i-j|}{L}\right)$.

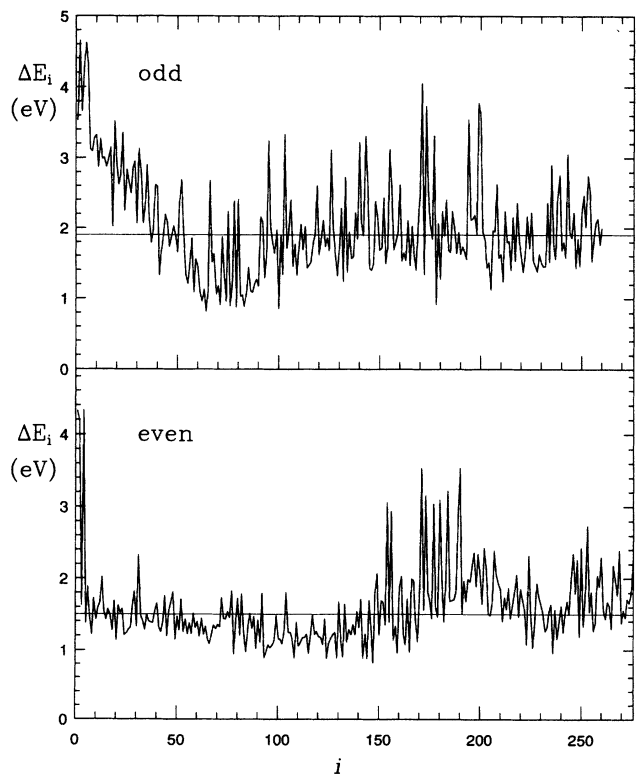

FIG. 21. Root-mean-square energy bandwidths for the odd and even matrices. Straight lines correspond to the average values of 1.9 eV (odd) and 1.5 eV (even).

It means that there is an obvious difference between the localization length L introduced to characterize the exponential localization of eigenstates in some of the models and the number of principal components N defined according to Eqs. (3.3)–(3.5). However, there is a different definition of L [18] that does not appeal to the character of the localization:

$$L_H = N_m \exp(H - H_{\mathrm{GOE}}) , \quad \text{(E2)}$$

$$\text{where} \quad H = -\sum_j C_j^2 \ln C_j^2 . \quad \text{(E3)}$$

Here N_m is the rank of the matrix, C_j are the components of a particular eigenstate, and H_{GOE} is the "entropy" (E3) calculated for the Gausian orthogonal ensemble (see [4] for detailed analysis of the GOE). L_H is called the *entropy localization length.* The factor $N_m \exp(-H_{\mathrm{GOE}})$, introduced into Eq. (E2) in [18] for normalization purposes, is equal to $\exp(2 - \mathcal{C} - \ln 2) \simeq 2.075$ for large rank matrices ($\mathcal{C}$ is the Euler constant).

In Fig. 22 the entropy localization length is presented for the odd $J = 4$ levels of Ce as a function of their energies. Also shown are the numbers of principal components for each tenth level (same as in Fig. 14), multiplied by a factor of 1.37. The agreement observed suggests that an approximate relation $L_H \sim 1.4N$ is valid.

If one assumes that the localization of the eigenstate is described by the mean square $\overline{C_j^2} \equiv w(E_j) = N^{-1} f\left(\frac{E_j - E}{\Gamma}\right)$ [see Sec. III B and Eq. (4.11)], and the distribution of the components is otherwise uncorrelated and Gausian [with the $w(E_j)$ variance around E_j], the entropy H can be calculated as follows:

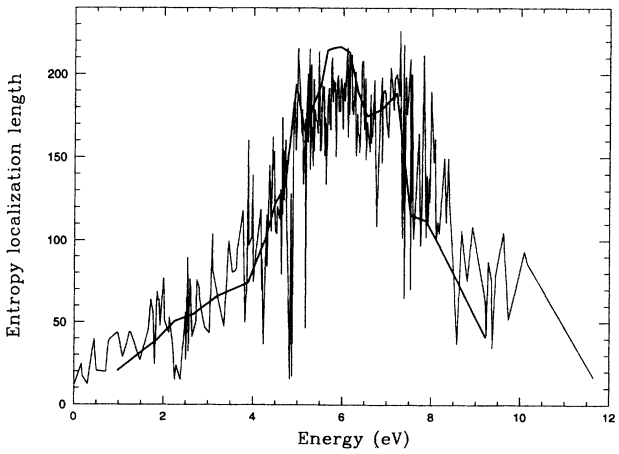

FIG. 22. Entropy localization length $L_H = 2.075 \exp(-\sum_j C_j^2 \ln C_j^2)$ for the odd Ce levels as a function of their energy. The thick curve is $1.37N$, where N is the number of principal components obtained from the Lorenzian fit.

$$H = -\int\int C^2 \ln C^2 \frac{1}{\sqrt{2\pi w(E_j)}} \times \exp\left(-\frac{C^2}{w(E_j)}\right) dC \frac{dE_j}{D}$$
$$= -(2 - \mathcal{C} - \ln 2) - \int w(E_j) \ln w(E_j) \frac{dE_j}{D} . \quad \text{(E4)}$$

The first item in Eq. (E4) cancels the normalization factor $N_m \exp(-H_{\rm GOE})$ in Eq. (E2). The entropy localization length is then given by

$$L_H = N \exp\left(-A^{-1} \int f(\epsilon) \ln f(\epsilon) d\epsilon\right) , \quad \text{(E5)}$$

where $A \equiv \int f(\epsilon) d\epsilon$. Both the integral in the exponent and A are model dependent. Equation (E5) yields the following relations: $L_H = 4N$, $2.16N$, and N for the Lorenzian, squared Lorenzian, and rectangular approximations for $f(\epsilon)$, respectively. Therefore, in principle, one can use the relation between L_H and N to distinguish between different types of localization. However, it would be prematurely to draw any conclusions from the fact that the "experimental" relation is $L_H \simeq 1.4N$ (Fig. 22), since neither the influence of the finite size of the matrix in the CI calculation nor the actual distribution of the components has been carefully checked yet.

If Gausian statistics are assumed for the components C_j at a given E_j, then the number of components in the interval dE_j falling into the $[C, C + dC]$ interval is

$$dN_{C,E_j} = \frac{1}{\sqrt{2\pi w(E_j)}} \exp\left\{-\frac{C^2}{w(E_j)}\right\} \frac{dE_j}{D} dC . \quad \text{(E6)}$$

The distribution of the components is then described by the following expression:

$$\frac{dN_C}{dC} = \int \frac{1}{\sqrt{2\pi w(E_j)}} \exp\left\{-\frac{C^2}{w(E_j)}\right\} \frac{dE_j}{D}$$
$$= \frac{N^{3/2}}{A\sqrt{2\pi}} \int \frac{1}{\sqrt{f(\epsilon)}} \exp\left\{-\frac{NC^2}{2f(\epsilon)}\right\} d\epsilon . \quad \text{(E7)}$$

It is again expressed in terms of the shape function $f(\epsilon)$. The Eq. (E7) reveals that $N^{-3/2}\frac{dN_C}{dC}$ is a universal function of the scaled variable $\tilde{C} = N^{1/2}C$:

$$N^{-3/2}\frac{dN_C}{dC} = \frac{1}{A\sqrt{2\pi}} \int \frac{e^{-\tilde{C}^2/2f(\epsilon)}}{\sqrt{f(\epsilon)}} d\epsilon . \quad \text{(E8)}$$

Therefore we can use the data obtained for the levels with different N to check the distribution of the components (Fig. 23) and thus make some conclusions about the localization shape $f(\epsilon)$.

An asymptotic form can be derived from Eq. (E8) at $\tilde{C} \gg 1$ ($C \gg N^{-1/2}$):

$$N^{-3/2}\frac{dN_C}{dC} \simeq \sqrt{\frac{2}{|f''(0)|}} \frac{e^{-\tilde{C}^2/2}}{A|\tilde{C}|} . \quad \text{(E9)}$$

In general, the weaker the localization, the sharper the

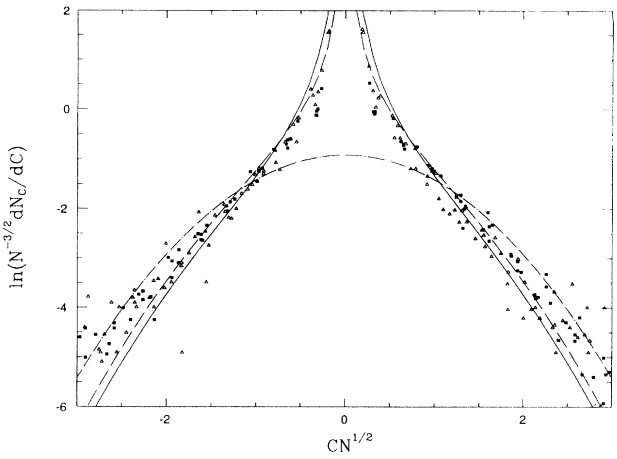

FIG. 23. The logarithm of the scaled distribution of the components C_j over the scaled $CN^{1/2}$ variable. Open triangles, odd levels 21–40 (N_{30} = 37), 41–60 (N_{50} = 42), 61–80 (N_{70} = 76), 81–100 (N_{90} = 104), and 101–120 (N_{110} = 126), solid squares, even levels 21–40 (N_{30} = 79), 41–60 (N_{50} = 107), 61–80 (N_{70} = 116), 81–100 (N_{90} = 116), and 101–120 (N_{110} = 121). Also shown are the scaled distributions corresponding to the Lorenzian localization (solid curve), squared Lorenzian localization (dashed curve), and "rectangular" localization (dash-dotted curve).

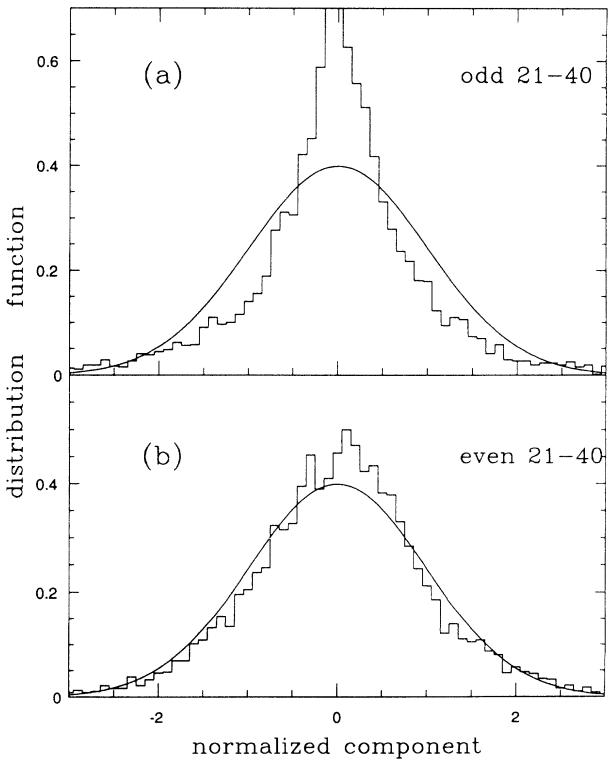

FIG. 24. The distributions of the normalized components $C_j^{(i)}\left[\left(C_j^{(i)}\right)^2\right]^{-1/2}$ for the 21–40 odd [histogram (a)] and even [histogram (b)] levels, compared with the Gaussian distribution (solid curves).

$f(\epsilon)$ maximum at $\epsilon = 0$ and the lower the curve predicted by Eq. (E9) goes (the numerical factors before $e^{-\tilde{C}^2/2}/|\tilde{C}|$ are $\sqrt{2}/\pi \simeq 0.45$ and $\pi^{-1} \simeq 0.318$ for the squared Lorenzian and Lorenzian $f(\epsilon)$, respectively). This behavior is qualitatively different from the simple Gaussian one, which takes place in the case of maximal quantum chaos (MQC) (which was assumed in [8]):

$$N^{-3/2}\frac{dN_C}{dC} = \frac{e^{-\tilde{C}^2/2}}{\sqrt{2\pi}} . \qquad \text{(E10)}$$

The MQC implies that each eigenstate has exactly N components — random Gausian variables with the variances equal to N^{-1} [8].

The numerical data presented in Fig. 23 were obtained in the form of histograms for several sets of 20 odd and even levels and rescaled to the $N^{-3/2}\frac{dN_C}{dC}$ function of the $\tilde{C}$ variable using the values of N from Figs. 14 and 15. It is compared with the model distribution (E8) calculated for the Lorenzian $[f(\epsilon) = (1 + 4\epsilon)^{-1}]$, squared Lorenzian $[f(\epsilon) = (1 + 4\epsilon)^{-2}]$, and rectangular $[f(\epsilon) = 1$ at $|\epsilon| \leq \frac{1}{2}$ and 0 elsewhere] localization shapes. The latter corresponds to the hypothesis of the MQC. It is the strongest type of localization conceivable. What prevents the numerically obtained points in Fig. 23 from following a unique curve is partly statistical fluctuations and partly the influence of the finite matrix size and the effects of selective configuration mixing (like that revealed in Appendix D). However, one can ascertain that, first, the scaling is indeed observed, and second, the localization is more diffuse than that of the MQC and stronger than that predicted by the Lorenzian model. Indirectly, it also supports the assumption of the approximate Gaussian distribution of the components C_j for the fixed basis state energy E_j or, more rigorously, for the fixed energy difference $|E_j - E^{(i)}|$ between the basis state and the eigenstate.

Finally we present a direct comparison of the components' distribution with the Gaussian one. In doing so the normalized components $C_j^{(i)}\left[\overline{\left(C_j^{(i)}\right)^2}\right]^{-1/2}$ were calculated in close analogy with the normalized matrix elements in Sec. IV B. Their distributions for the 21st to 40th odd and even levels are shown in Figs. 24(a) and 24(b), respectively. Apparently, one can speak of good agreement with the Gaussian statistics for the latter, whereas in the former case the calculated distribution greatly exceeds the Gaussian one at small values of the variable (< 0.5) as well as at large ones (> 2.5). This difference accords with the previous observation about the emergence of chaos in the odd and even manifolds (see Secs. II B and II C). We checked that for the 100th to the 120th odd and even levels the distributions of the normalized components become much more alike. However, a statistically significant deviation from the Gaussian distribution, like that in Fig. 24(b), still holds for them. It makes the situation similar to that observed in Fig. 17 for the normalized matrix elements. Gaussian statistics appear to be a limiting case which may be achieved only when complete chaotic mixing takes place. In a real system there may always be present the perturbation theory contributions (small though not statistical) due to the selective mixing of some particular basis states.

[1] V. Flambaum, G. Gribakin, and M. Kozlov, Bull. Am. Phys. Soc. **38**, 1111 (1993).

[2] W. C. Martin, R. Zalubas and L. Hagan, *Atomic Energy Levels — The Rare-Earth Elements*, Natl. Bur. Stand. Ref. Data Ser., Natl. Bur Stand. (U.S.), NBS-60, (U.S, GPO, Washington, DC, 1978).

[3] A. Bohr and B. Mottelson, *Nuclear Structure* (Benjamin, New York, 1969), Vol. 1, Chap. 2.

[4] T. A. Brody, J. Flores, J. B. French, P. A. Mello, A. Pandey, and S. S. M. Wong, Rev. Mod. Phys. **53**, 385 (1981).

[5] H. C. Camarda and P. D. Georgopulos, Phys. Rev. Lett. **50**, 492 (1983).

[6] O. P. Sushkov and V. V. Flambaum, Pis'ma Zh. Eskp. Teor. Fiz. **32**, 377 (1980) [JETP Lett. **32**, 353 (1980)].

[7] R. Haas, L. B. Leipuner, and R. K. Adair, Phys. Rev. **116**, 1221 (1959); R. J. Blin-Stoyle, *ibid.* **120**, 181 (1960); I. S. Shapiro, Usp. Fiz. Nauk **95**, 647 (1968) [Sov. Phys. Usp. **11**, 682 (1969)].

[8] B. V. Chirikov, Phys. Lett. **108A**, 68 (1985).

[9] F. M. Izrailev, Phys. Rep. **196**, 299 (1990).

[10] G. Casati, B. V. Chirikov, I. Guarneri, and F. M. Izrailev, Phys. Rev. E **48**, R1613 (1993).

[11] E. P. Wigner, Ann. Math. **62**, 548 (1955); **65**, 203 (1957).

[12] Y. V. Fyodorov and A. D. Mirlin, Phys. Rev. Lett. **69**, 1093 (1992).

[13] V. A. Dzuba, V. V. Flambaum, and I. B. Khriplovich, Z. Phys. D **1**, 243 (1986).

[14] A. A. Radtsig and B. M. Smirnov, *Parameters of Atoms and Atomic Ions: Handbook* (Energoatomizdat, Moscow, 1986).

[15] I. I. Tupizin kindly supplied us with his original HFD and CI codes. The description of the HFD code is given in V. F. Brattsev, G. B. Deineka, and I. I. Tupitsyn, Izv. Akad. Nauk SSSR **41**, 2655 (1977) [Bull. Acad. Sci. USSR, Phys. Ser. (USA) **41**, 173 (1977)], and the references to the CI code can be found in S. A. Kotochigova and I. I. Tupizin, J. Phys. B **20**, 4759 (1987).

[16] V. A. Dzuba, V. V. Flambaum, P. G. Silvestrov, and O. P. Sushkov, J. Phys. B **20**, 1399 (1987) (core polarization effects in Tl and Au); Phys. Lett. A **131**, 461 (1988) (screening of the Coulomb interaction); Phys. Rev. A **44**, 2828 (1991) (many-body perturbation theory applied to the open-shell atoms of Pb and Bi); V. A. Dzuba, V. V. Flambaum, and O. P. Sushkov, Phys. Lett. A **140**, 493 (1988) (calculation of Cs energy levels with 0.1% accuracy).

[17] M. Feingold, D. M. Leitner, and M. Wilkinson, Phys. Rev. Lett. **66**, 986 (1991).

[18] G. Casati, L. Molinari, and F. Izrailev, Phys. Rev. Lett.

64, 1851 (1990); J. Phys. A **24**, 4755 (1991).
[19] V. V. Flambaum, Phys. Scr. **T46**, 198 (1993).
[20] V. V. Flambaum and O. K. Vorov, Phys. Rev. Lett. **70**, 4051 (1993).
[21] V. V. Flambaum, in *Time Reversal Invariance and Parity Violation in Neutron Reactions*, edited by C. R. Gould, J. D. Bowman, and Yu. P. Popov (World Scientific, Singapore, 1994), p. 39.
[22] I. B. Khriplovich, *Parity Nonconservation in Atomic Phenomena* (Gordon and Breach, Philadelphia, 1991).
[23] I. S. Gradshteyn and I. M. Ryzhik, in *Tables of Integrals, Series and Products*, edited by A. Jeffrey (Academic, New York, 1980).

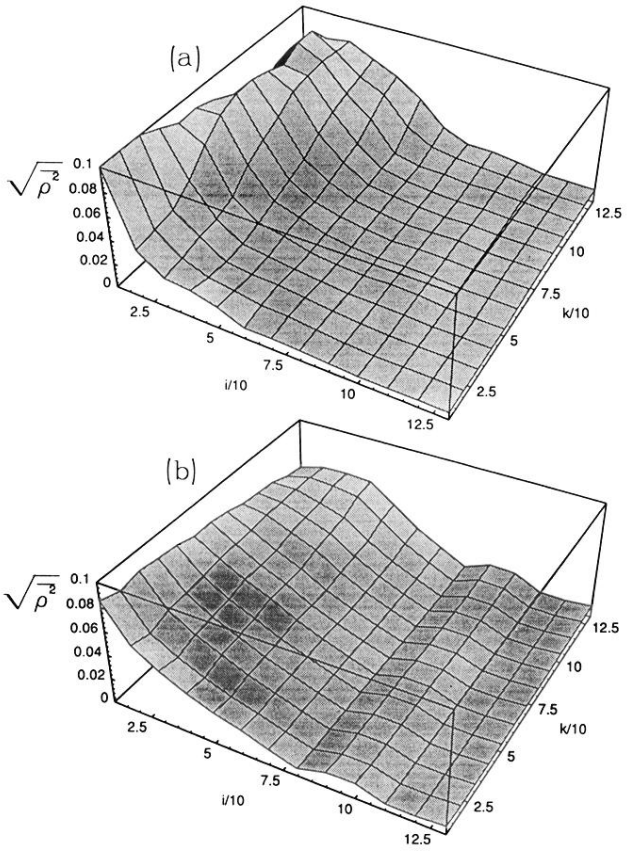

FIG. 16. Comparison of the numerical calculation of the matrix elements between the chaotic states with the results of the statistical theoretical approach. Shown is the dependence of the root-mean-squared matrix elements of the reduced density matrix operator $\left[\frac{2j+1}{2J+1}\overline{\left(\rho^{(ik)0}_{6s_{1/2}6p_{1/2}}\right)^2}\right]^{1/2}$ ($j = 1/2,\ J = 4$) on the ordinal numbers of the odd (i) and even (k) levels. (a) Window-averaged matrix elements from the CI calculations and (b) obtained from Eq. (4.21a).

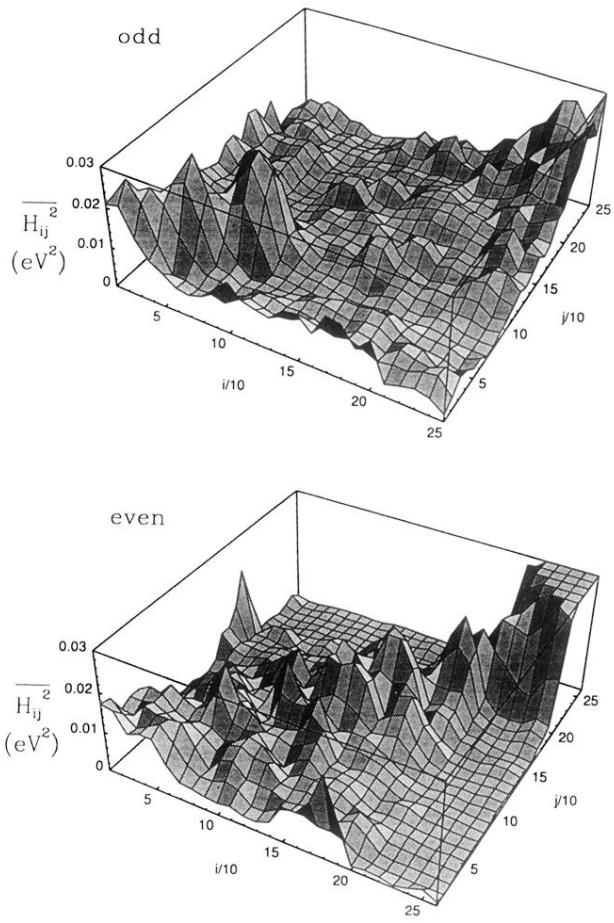

FIG. 9. The dependence of the mean-squared nondiagonal matrix element $\overline{H_{ij}^2}$ on the basis states' numbers i and j for the $J^\pi = 4^-,4^+$ Hamiltonian matrices (the 19×19 window averaging used). The values averaged over the whole matrix are 0.0072 eV^2 (odd) and 0.0076 eV^2 (even).